CANCER

A somatic mutation in moesin drives progression into acute myeloid leukemia

Ouyang Yuan[1]*, Amol Ugale[1,2], Tommaso de Marchi[3], Vimala Anthonydhason[4],
Anna Konturek-Ciesla[1], Haixia Wan[1], Mohamed Eldeeb[1], Caroline Drabe[1], Maria Jassinskaja[1,5],
Jenny Hansson[1], Isabel Hidalgo[1], Talia Velasco-Hernandez[6], Jörg Cammenga[1],
Jeffrey A. Magee[7,8], Emma Niméus[3,9], David Bryder[1]*

Acute myeloid leukemia (AML) arises when leukemia-initiating cells, defined by a primary genetic lesion, acquire subsequent molecular changes whose cumulative effects bypass tumor suppression. The changes that underlie AML pathogenesis not only provide insights into the biology of transformation but also reveal novel therapeutic opportunities. However, backtracking these events in transformed human AML samples is challenging, if at all possible. Here, we approached this question using a murine in vivo model with an MLL-ENL fusion protein as a primary molecular event. Upon clonal transformation, we identified and extensively verified a recurrent codon-changing mutation (Arg^{295}Cys) in the ERM protein moesin that markedly accelerated leukemogenesis. Human cancer-associated moesin mutations at the conserved arginine-295 residue similarly enhanced MLL-ENL–driven leukemogenesis. Mechanistically, the mutation interrupted the stability of moesin and conferred a neomorphic activity to the protein, which converged on enhanced extracellular signal–regulated kinase activity. Thereby, our studies demonstrate a critical role of ERM proteins in AML, with implications also for human cancer.

INTRODUCTION

Acute myeloid leukemia (AML) arises from genetic and/or epigenetic events in immature hematopoietic cells that lead to the formation of leukemia-initiating cells (LICs) (1). LICs gain a competitive advantage over normal hematopoietic progenitors and progress into AML upon additional genetic perturbations that further promote proliferation and/or inhibit differentiation (1–3). The identity of secondary mutations can thereby shed light on the biology of leukemic transformation and provide molecular candidates for therapeutic targeting.

Balanced chromosomal translocations that involve the mixed lineage leukemia–1 (MLL1/KMT2A) gene can form chimeric fusion proteins with novel gene regulatory properties. These MLL rearrangements (MLLr) represent recurrent initiating events in AML and comprise 35 to 50% of AML cases in infants (4). In older children and adults, MLLr can be found in ~3% of de novo AML cases (5). In general, MLLr AML associate with a poor prognosis (6) and a substantial fraction of these leukemias harbor somatic mutations believed to drive transformation, with activating mutations in RAS, FLT3, PTPN11, and BRAF being the most common (5). This has lent support to a two-step model of leukemogenesis in which the initial MLLr act to mainly inhibit differentiation and the secondary mutations

activate signals that drive proliferation, without excluding that the secondary mutations can also contribute to enhanced survival and/or further inhibit differentiation. However, in pediatric MLLr acute lymphoblastic leukemia (ALL), the frequency of secondary mutations is lower and these mutations are often subclonal and frequently lost upon relapse (7). This has challenged the generality of the two-step model of MLLr leukemia by suggesting that these fusion products can drive leukemia by itself in a target cell-dependent manner and/or that genetic predisposition can replace for somatically acquired secondary mutations.

The powerful oncogenic activity of MLL fusion proteins has been frequently exploited in mouse models to explore the pathogenesis of leukemic initiation, evolution, therapy resistance, and relapse. In most of such work, MLL fusions have been introduced by viral delivery to immature murine hematopoietic cells, followed by their transplantation into recipient mice (8). Using these approaches, a few recent attempts have been made to map secondary mutations in MLL-AF9–driven AML (9, 10). Consistent with data from human patients, there have been reports on secondary genetic/activating lesions in KRAS, BRAF, CBL, PTPN11, and GNB2 upon transformation. In support of the relevance of these mutations for AML development, their coexpression with different MLL fusions can accelerate leukemogenesis and produce more aggressive and rapid AML (9, 11, 12). However, substantial differences exist between mutation patterns in human leukemic samples and the few murine studies executed to date. Most notably, these differences relate to the exact types of secondary mutations identified and their observed frequencies, with extensive subclonality observed in murine studies. While this obviously could be a real observation, the possibility remains that the modeling of leukemia initiation in murine models does not accurately reflect the monoclonality of human AML.

As an alternative to viral delivery, we previously generated an inducible transgenic mouse strain in which a human MLL-ENL fusion gene can be induced by doxycycline (iMLL-ENL mice) (13). The rationale for this approach was to circumvent several of the

[1]Division of Molecular Hematology, Department of Laboratory Medicine, Lund Stem Cell Center, Faculty of Medical, Lund University, 221 84 Lund, Sweden. [2]Department of Microbiology, Immunobiology and Genetics, Center for Molecular Biology of the University of Vienna, Max F. Perutz Laboratories, Vienna Biocenter (VBC), 1030 Vienna, Austria. [3]Division of Surgery, Oncology, and Pathology, Department of Clinical Sciences, Lund University, Solvegatan 19, 223 62, Lund, Sweden. [4]Sahlgrenska Center for Cancer Research, University of Gothenburg, Medicinaregatan 1F, 413 90, Gothenburg, Sweden. [5]York Biomedical Research Institute, Department of Biology, University of York, Wentworth Way, York YO10 5DD, UK. [6]Josep Carreras Leukaemia Research Institute, 08036 Barcelona, Spain. [7]Department of Pediatrics, Division of Hematology and Oncology, Washington University School of Medicine, St. Louis, MO 63110, USA. [8]Department of Genetics, Washington University School of Medicine, St. Louis, MO 63110, USA. [9]Department of Surgery, Skåne University Hospital, Entrégatan 7, 222 42 Lund, Sweden.
*Corresponding author. Email: ouyang.yuan@med.lu.se (O.Y.); david.bryder@med.lu.se (D.B.)

experimental caveats associated with viral delivery of MLL fusions, including poor delivery, unphysiological expression levels caused by the strong promoters typically associated with viral vectors, and insertional mutagenesis. In addition, the iMLL-ENL model has allowed us to firmly establish the precise identity of hematopoietic progenitor cells capable of initiating AML, without having to subject candidate cells to any form of in vitro culture before assessment of their leukemic capacity (*13*, *14*).

Here, we set out to dissect the stepwise AML progression in the iMLL-ENL model. We demonstrate a three-phase progression of evolving AML, in which preleukemic cells initially expand, which was followed by a contraction and later transformation into AML in a clonal-dependent manner. To clarify the molecular pathogenesis that drives the transformation process, we subjected multiple independent AMLs to exome sequencing. This revealed a highly recurrent de novo mutation in the X-linked ezrin-radixin-moesin (ERM) protein moesin that leads to cysteine change at the evolutionary conserved arginine-295 residue. Detailed functional studies revealed that R295C mutant MSN markedly accelerated leukemogenic transformation, with human cancer-associated mutations at the same residue having similar effects on the transformation process. Thereby, our work provides new insights into the molecular pathogenesis of disease progression in *MLL*r AML.

RESULTS

A triphasic and monoclonal disease pattern underlie transformation into MLL-ENL–driven AML

To explore mechanisms underlying development into AML, we used a transplantation-based mouse model in which a human *MLL-ENL* fusion gene can be conditionally induced in defined murine LICs by administration of doxycycline (*13*). We previously showed that myeloid-oriented pre-granulocyte/macrophage progenitors (pGMs; Lin$^-$Sca1$^-$kit$^+$CD41$^-$CD150$^-$CD105$^-$) are potent LICs in the iMLL-ENL model (*13*). Building on these previous observations, we isolated pGMs from iMLL-ENL mice and transplanted the cells into wild-type (WT) recipients under continuous doxycycline/MLL-ENL induction. The use of different congenic CD45 markers allowed for monitoring of transplanted cells and host/competitor cells in peripheral blood (PB) over time.

We observed a pattern of leukemic development in which MLL-ENL–induced pGM cells initially (4 weeks after transplantation) yielded a high level of myeloid contribution in transplanted hosts (Fig. 1A). WT pGMs provide only marginal, if any, myeloid reconstitution at this point (*15*). After this, we observed declines in myeloid contribution, which was consistent among individual hosts but varied between mice as for magnitude (Fig. 1A). Later, we observed rapid rebounds in iMLL-ENL–derived myeloid cells that continued to elevate (Fig. 1A) and coincided with AML diagnosis according to the Bethesda classification for murine myeloid malignancies (*16*). Compared to retroviral MLL-fusion models, the initial (pre)leukemogenic pattern from iMLL-ENL cells was different, in that (pre)leukemogenic cells with retrovirally delivered *MLLr* appear to continuously elevate following their initial detection (*17*).

In most murine AML models, including the iMLL-ENL model, AML is initiated from a pool of candidate LICs (*18*). However, human AML typically have a monoclonal origin (*1*). This led us to next investigate the clonal composition of AMLs developing from iMLL-ENL LICs. For this, we transduced iMLL-ENL LICs immediately after

their isolation with a lentiviral barcode library (*19*) and transplanted the cells as before into WT recipients under MLL-ENL induction (Fig. 1B). Upon disease, we extracted genomic DNA (gDNA) from donor-derived AML cells, which was followed by Sanger sequencing of the introduced barcodes. In four of the six analyzed leukemic samples, we recovered a single dominant barcode (Fig. 1B). In the remaining two cases, we observed a more crowded barcode sequence, indicating either a polyclonal origin or possibly a leukemic clone that originally was provided with more than one barcode (Fig. 1B). Together, these results demonstrated selection and evolution of predominant/driver clones during the development of murine MLL-ENL–driven AML, a similarity to that observed in human patients.

iMLL-ENL AMLs associate with a highly recurrent point mutation in the X-linked gene moesin that leads to an arginine-295–to–cysteine substitution

Given the pattern of leukemic development in the AML model (Fig. 1), we hypothesized that transformation into AML associate with the acquisition of secondary driver mutations. We therefore next set out to identify these mutations.

We previously showed that AML can originate from several different types of hematopoietic progenitor cells in the iMLL-ENL model, including common lymphoid progenitors (CLPs; Lin$^-$IL7Ra$^+$Flt3$^+$Sca1^{low}c-kit^{low}), granulocyte-macrophage-lymphoid progenitors (GMLPs; Lin$^-$Sca1$^+$ckit$^+$CD48$^+$CD150$^-$: these cells are mostly positive for CD34 and Flt3), and pGMs (*13*). Building on this and to explore whether any distinct secondary mutation patterns might associate with different cell types of origin (for instance, related to inherent differences in proliferation or lineage potential), we designed a first experiment where we assessed secondary somatic driver mutations in AML samples derived from different LIC types. We isolated CLPs, GMLPs, and pGMs from iMLL-ENL mice and transplanted the cells to new recipients in conjunction with induction of MLL-ENL. Upon transformation, we isolated gDNA from leukemic cells and subjected samples to exome sequencing (the general strategy for detection of secondary mutations is outlined in Fig. 2A). Following filtering (see methods for details), we could extract 40 candidate somatic variants in this first experiment, out of which nine mutations were recurrent (Fig. 2B and table S1). From subsequent sequencing experiments (below), three of these mutations (in *Flrt1*, *Polr3e*, and *Mcts2*) could be classified as germline rather than somatic. Out of the other six recurrent mutations, only a C883T mutation in moesin was confirmed as somatically acquired at high variant allele frequency (VAF) (>0.3) and across multiple samples. This mutation leads to an amino acid change of arginine-295 to cysteine (R295C).

To extend our first sequencing experiment, we focused on AML derived from pGM cells. This is because of the similarity in mutation spectra across initiating cell types in our first experiment (Fig 2B and fig. S1) and because pGM are more easily accessible/frequent than GMLPs and CLPs. In subsequent experiments, we also redesigned our approach slightly such that AML was initiated from individual mice for which we, at initiation of experimentation, also generated appropriately matched/paired control samples. This was done to identify somatic mutations acquired upon AML transformation more easily. Thus, we conducted three additional sequencing experiments in which three separate founder mice were used to generate 13 additional leukemic samples (3 AML samples from founder 2, 6 AML samples from founder 3, and 4 AML samples from founder 4). The only recurrently mutated genes across these three cohorts were *Msn*
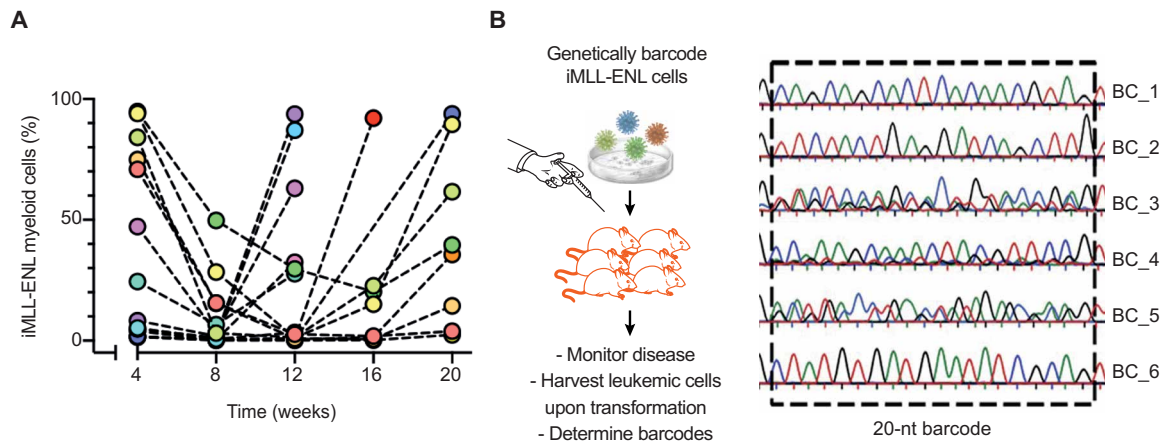
Fig. 1. Disease characteristics of the iMLL-ENL model. (**A**) pGMs were isolated from iMLL-ENL mice and transplanted competitively into lethally irradiated recipients (*n* = 10). Colored symbols and connecting lines show levels of donor-derived myeloid in individual recipients over time. (**B**) Left: Strategy used to evaluate the clonal composition of iMLL-ENL transformed AML using lentiviral barcoding. Right: Sanger sequencing of DNA barcodes after transformation, demonstrating clonality in a majority of individual AMLs.

(9 of 13 samples) and *Ptpn11* (2 of 13, G60V and E76K) (Fig. 2C). Taking all four cohorts (22 sequenced AML samples) into account, the R295C *Msn* mutation was by far the most frequently secondary mutation (detected in 14 samples). Other recurrently mutated genes were *Ptpn11* (3), *Cdh11* (3), *Cdk4* (2), *Fbxo22* (2), *Sh2d1b1* (2), and *Exo1* (2) (fig. S1). *Ptpn11* and *Cdk4* mutations have been shown previously to activate RAS signaling and cell cycle regulation, respectively, in human AML (*11*, *20*). Single-mutant cases were observed for several genes (fig. S1 and table S1), including for instance in *Hras* and *Braf*, that have also previously been reported to be mutated in AML (*6*, *10*, *11*, *20–31*). Last, to determine whether the C883T/R295C was dependent on the transplantation setting, we interrogated 10 separate iMLL-ENL AML samples derived from an alternative, non–transplantation-based model system (*32*). We observed a high frequency (7 of 10) of the C883T/R295C *Msn* mutation also in these samples (Fig. 2D).

We previously observed that pGM cells give rise to a small fraction of lymphoid cells upon transplantation (*15*). To further confirm the specificity of the C883T/R295C *Msn* mutation to AML, we isolated donor-derived T and B cells at the same time as AML cells and subjected gDNA from these cell subsets to Sanger sequencing. This revealed the presence of the mutation only in the fraction of AML cells (Fig. 2E).

The *Msn* gene is located on the X chromosome. Given the very high VAF of the C883T/R295C mutation in male AML cells (Fig. 2, B to D), the observed mutation presented as hemizygously dominant in male leukemic cells. To extend our interrogations to female cells, we applied Sanger sequencing for both gDNA and cDNA from female leukemic samples (the AML samples of experiment pGM_2 in Fig. 2C). Both WT *Msn* and the mutant C833T/R295C allele could be retrieved in gDNA from samples in which the mutation had been detected by Illumina sequencing (Fig. 2F). By contrast, only the mutant *Msn* allele could be detected upon analysis of cDNA (Fig. 2F). This demonstrated that the mutant allele localizes to the active X chromosome in female cells.

Given the high recurrence of the C833T/R295C *Msn* mutation, we hypothesized that this mutation perhaps could be somatically acquired in a small fraction of hematopoietic cells as part of normal mouse biology and that the onset of MLL-ENL expression might

select for such cells. This hypothesis was further entertained by the detection of a low VAF of the mutation in one of the founder mice (Fig. 2C and table S1). To explore this possibility, we performed ultradeep targeted sequencing of hematopoietic progenitors isolated from both WT C57BL/6 and uninduced iMLL-ENL mice (three individual mice per genotype). As controls for the detection sensitivity, we used synthesized oligonucleotide templates of either WT, 0.1%, or 1% spike-in C833T/R295C mutant *Msn* sequences. With an average sequencing depth of approximately 40,000 reads per sample (table S2), we could recover 0.12 and 0.88% mutant sequences in the 0.1 and 1% spike-in controls, respectively. However, the frequency of C833T substitution in WT C57BL/6 or uninduced iMLL-ENL samples was not higher than the negative (WT) controls (Fig. 2G).

Collectively, while our attempts to identify relevant driver mutations revealed that MLL-ENL–driven murine AMLs associate with few dominant and recurrent secondary mutations (table S1), which seem to be in agreement with the situation also in human *MLL* fusion–driven leukemia (*7*, *31*, *33*), one notable exception was a C833T mutation in the *Msn* gene that leads to an R295C substitution. This mutation was found in 21 of 32 (65.6%) of the AML samples evaluated by exome sequencing and mostly at high VAF, without any apparent restriction as for cell of origin or to the transplantation setting. This X-linked mutation was further found to associate with the active X chromosome and to form in response to MLL-ENL expression, rather than existing as a preexisting somatic mutation subsequently selected for by coexpression of MLL-ENL.

C295 mutant MSN leads to a marked acceleration of AML progression

Given the high recurrence of the C295 MSN mutation (Fig. 2), we wanted to determine whether this mutation had any functional consequences on AML progression and/or propagation. For this, we transplanted iMLL-ENL LICs transduced with either WT or C295 mutant MSN into lethally irradiated congenic recipients and assessed leukemic progression (Fig. 3A). We observed that mice transplanted with C295 mutant MSN developed AML with a notably shortened latency (median latency, 28 days) compared to LICs with WT MSN (median latency, 90 days; Fig. 3B).
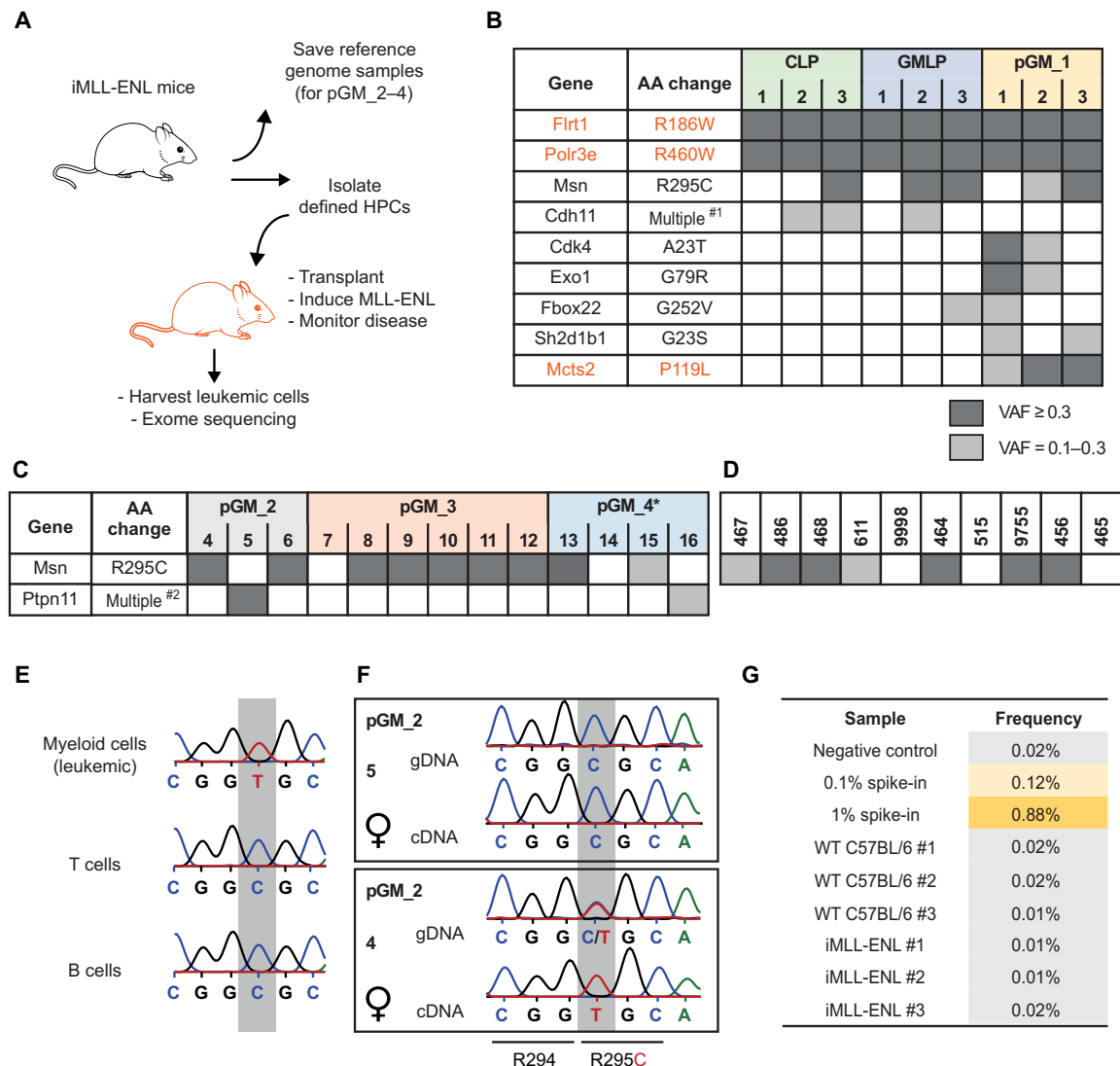
Fig. 2. iMLL-ENL cells associate with a recurrent codon-changing point mutation in moesin upon AML transformation. (**A**) Experimental strategy to identify secondary mutations that associate with transformation into MLL-ENL–driven AML. (**B**) Predicted deleterious mutations identified in AML samples originating from different LIC subsets. (#1) Three different missense variants were detected in *Cdh11*: p.G86V, p.I100F, and p.V147D. AA, amino acid. (**C**) The presence of the MSN R295C mutation in AML samples derived from pGM cells from three separate founders. (#2) Two different missense variants were detected in *Ptpn11*: p.G60V and p.E76K. *The founder mouse in pGM_4 was found to harbor a low AF of the MSN R295C mutation. (**D**) The presence of the MSN R295C mutation in AML samples derived from a non–transplantation-based model system. In (B) to (D), each column represents an individual leukemic sample, with dark gray boxes indicating a gain of mutation with an allele frequency (AF) > 0.3 and light gray boxes indicating a gain of mutation with an AF of 0.1 to 0.3. (**E**) Sanger sequencing chromatograms depicting the Msn missense C>T mutation (leading to the R295C substitution) in leukemic cells and in B and T cells from the same sample. (**F**) Sanger sequencing of *Msn* from gDNA and cDNA from two female leukemic samples derived from the same founder mouse, demonstrating that, in Msn mutant cells (experiment pGM_2, mouse 4), Msn expression is derived from the active X chromosome in female cells. The same results were obtained from AML sample mouse 6 in experiment pGM_2, which also presented with the *Msn* mutation. (**G**) Ultradeep targeted sequencing results of the *Msn* C883T substitution in WT C57BL/6 and uninduced iMLL-ENL cells.

To further characterize the influence of the C295 mutant MSN upon AML progression, we analyzed PB, bone marrow (BM), and spleen at 14, 21, and 28 days after transplantation of iMLL-ENL LICs ± C295 mutant MSN (Fig. 3, C to E). We observed that C295 mutant MSN increased the engraftment in a time-dependent manner in PB (Fig. 3C). This co-occurred with marked increases in spleen sizes (Fig. 3D). Morphological analyses showed that the frequency of leukemic blasts/undifferentiated cells derived from C295 mutant MSN LICs was significantly higher than that observed from WT MSN LICs and increased gradually after transplantation (Fig. 3D and fig. S2A). Fluorescence-activated cell sorting (FACS) analysis for the differentiation-associated markers CD36 and Gr1 revealed lower expression on C295 MSN mutant AML cells (fig. S2B). Quantitative reverse transcription polymerase chain reaction (qRT-PCR) demonstrated that iMLL-ENL cells with WT MSN exhibited reduced expression of the MLL-fusion AML-associated genes *Hoxa9* and *Meis1* over time. By contrast, C295 mutant MSN sustained high expression of these genes (fig. S2C).
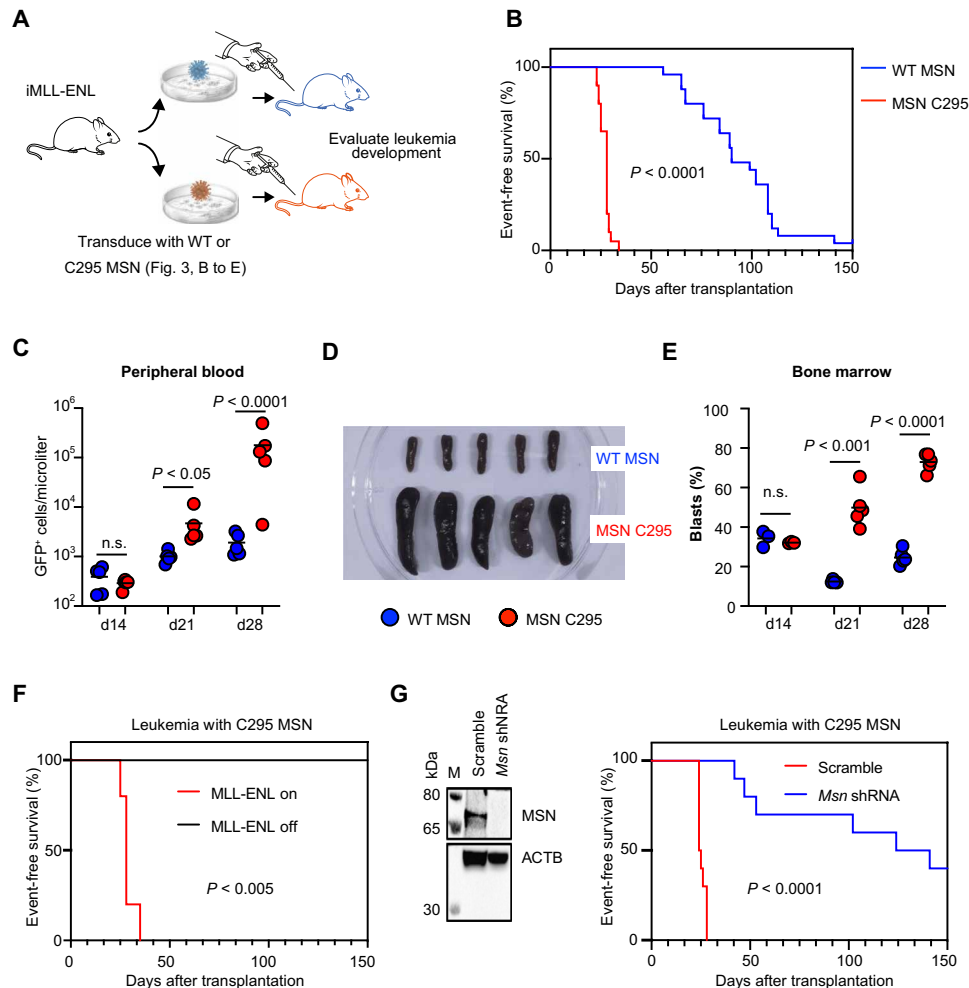
Fig. 3. AML progression is markedly accelerated by C295 mutant MSN and associates with diminished differentiation. (**A**) Outline of the experimental strategy used to explore the kinetics of MLL-ENL–driven AML development as a consequence of C295 mutant MSN. (**B**) Kaplan-Meier survival curves depicting event-free survival of recipients transplanted with iMLL-ENL LICs transduced with either WT ($n = 25$) or C295 mutant MSN ($n = 20$). (**C**) Count of green fluorescent protein–positive (GFP+) cells (transduced LICs) in PB of recipients at 14, 21, or 28 days after transplantation ($n = 5$ mice per group/time point). n.s., not significant. (**D**) Rapid development of spleno-megaly in recipients transplanted with C295 mutant MSN LICs. The image show spleens harvested from recipients 28 days after transplantation. (**E**) Blast cell frequency at 14, 21, and 28 days after transplantation of iMLL-ENL LICs with WT or C295 mutant MSN ($n = 5$ mice per group/time point). See also fig. S2. (**F**) AML with C295 mutant MSN continues to rely on MLL-ENL expression. Event-free survival of secondary recipients of iMLL-ENL and C295 mutant MSN expressing leukemic cells as a consequence of MLL-ENL expression ($n = 5$ mice per group). (**G**) Knockdown of C295 mutant MSN restricts the propagation of MLL-ENL–driven AML. Left: MSN expression was measured by Western blot following short hairpin RNA (shRNA)–mediated *Msn* knockdown. Right: Event-free survival in secondary recipients of MLL-ENL + C295 mutant MSN fol-lowing shRNA-mediated *Msn* knockdown ($n = 10$ per group). A scrambled shRNA was used as control. ACTB, beta-actin.

Because of the high pathogenicity of C295 mutant MSN, we next tested whether MLL-ENL leukemic blasts with C295 mutant MSN remained dependent on MLL-ENL expression. For this, we trans-planted C295 mutant MSN leukemic blasts to secondary hosts in the presence or absence of MLL-ENL expression. All mice with MLL-ENL induction presented with AML within 4 weeks, while mice without MLL-ENL induction showed no signs of disease develop-ment (Fig. 3F).

To determine the role of C295 mutant MSN for AML maintenance, we applied a short hairpin RNA (shRNA) approach. After verifica-tion of an effective shRNA that targets *Msn* (Fig. 3G, left), we intro-duced it to C295 MSN–bearing MLL-ENL AML cells and evaluated AML propagation in secondary hosts. Reducing the expression of C295 mutant MSN significantly impaired AML cell repopulation and

delayed AML progression (Fig. 3G, right). Together, these data demon-strate that the C295 MSN mutation collaborate with MLL-ENL to promote a rapid transformation into AML that is characterized by a pronounced inhibition of differentiation.

C295 mutant MSN does not affect normal hematopoiesis
Having established a potent leukemia-promoting activity of the C295 MSN variant (Fig. 3), we next explored the influence of the mutant protein on normal hematopoiesis. For this, we transduced normal candidate hematopoietic stem cells (HSCs) with either WT or C295 mutant MSN, which was followed by competitive trans-plantation. We observed a highly similar multilineage contribution from WT or C295 MSN–transduced HSCs (Fig. 4A), without any apparent signs of disease development. This suggested that the

C295 MSN mutation is not pathogenic by itself but rather a cooperating event with MLL-ENL.

MSN is dispensable for MLL-ENL AML and its effects are independent on T558 phosphorylation

In a next set of experiments, we investigated whether MSN function was essential for the initiation of MLL-ENL leukemogenesis. For this, we reduced normal *Msn* expression in iMLL-ENL LICs before their transplantation. In this setting, disease latency was indistinguishable

between LICs carrying the scramble shRNA and the *Msn* shRNA (Fig. 4B).

It is well established that phosphorylation of MSN threonine-558 (T558) plays a crucial role for the activity of MSN (*34*). To investigate whether this phosphorylation might play a role in AML development, we transplanted iMLL-ENL LICs with phosphoinactive (T558A) or phosphomimetic (T558D) MSN variants (*34*) and assessed leukemic progression. Somewhat unexpectedly, these two variants did not differ as for disease latency (Fig. 4C). Next, we investigated the
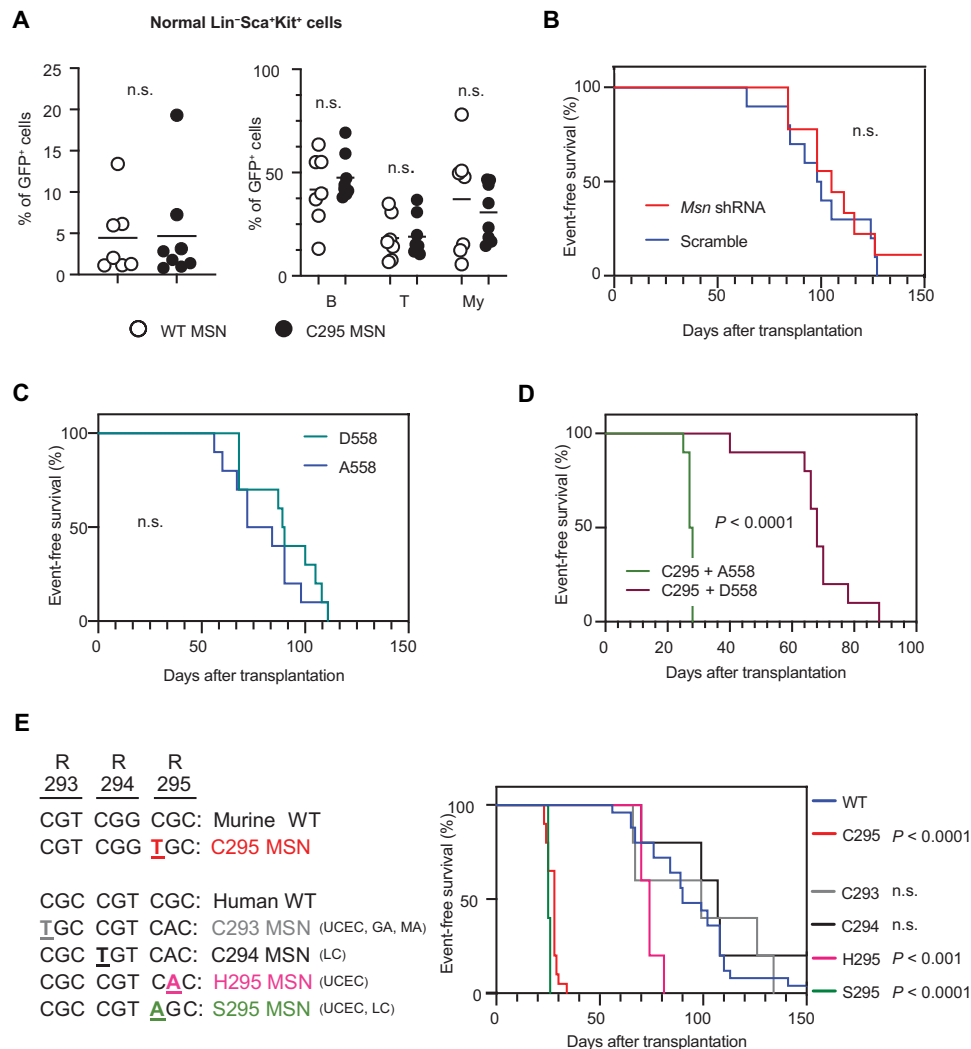

Fig. 4. Human cancer-associated *MSN* mutations accelerate AML progression. (**A**) The C295 mutant MSN does not affect normal HSC function or multilineage development. Left: Engraftment of normal candidate HSCs expressing WT or C295 mutant MSN (GFP$^+$) in PB at 28 weeks after transplantation. Right: Hematopoietic lineage distribution from WT or C295 mutant MSN (*n* = 7 to 8 mice per group). (**B**) MSN is dispensable for disease progression from iMLL-ENL LICs. Kaplan-Meier survival curves depict event-free survival of recipients transplanted with iMLL-ENL LICs transduced with either a scramble shRNA or an shRNA against *Msn* (*n* = 10 mice per group). (**C**) Event-free survival of recipients transplanted with iMLL-ENL LICs transduced with either a phosphoinactive mutant construct (MSN T558A) or a phosphomimetic mutant (MSN T558D) (*n* = 10 mice per group). (**D**) Leukemic propagation of C295 mutant MSN AML is impaired by the phosphomimetic T558D mutation. Kaplan-Meier survival curves depict event-free survival of recipients transplanted with iMLL-ENL LICs expressing C295 MSN together with either phosphoinactive T558A (C295 + A558) or phosphomimetic T558D (C295 + D558) variants (*n* = 10 mice per group). (**E**) R295 mutant MSN-variants identified in human cancers accelerate MLL-ENL–driven AML progression. Left: MSN variants adjacent to the R295 residue from The Cancer Genome Atlas (TCGA) and Catalog of Somatic Mutations in Cancer databases. UCEC, uterine corpus endometrial carcinoma; GA, gastric adenocarcinoma; MA, melanoma; LC, large intestine carcinoma. Right: Kaplan-Meier survival curves depict event-free survival of recipients transplanted with iMLL-ENL LICs transduced with C293, C294, H295, or S295 MSN variants (*n* = 5 per group). iMLL-ENL LICs cells transduced with WT or C295 MSN (same as in Fig. 3B) are included for reference.

potential role of the phosphorylation status of T558 on C295 mutant MSN. For this, we generated compound mutant variants of C295 MSN together with the phosphoinactive T558A (C295 + A558) or phosphomimetic T558D (C295 + D558) variants. Notably, mice receiving LICs transduced with the phosphomimetic C295 + D558 MSN developed AML with a significantly longer latency (median, 68 days) compared to mice receiving cells transduced with the phosphoinactive C295 + A558 MSN (median, 28 days; $P < 0.0001$; Fig. 4D).

Together, modulation of the phosphorylation status of WT MSN at T558 had little effect on the latency of MLL-ENL–driven transformation. This was markedly different in the context of the C295 mutation, where mimicking T558 phosphorylation abrogated most of its leukemia-propagating activity.

Human cancer-associated MSN mutations at the R295 residue accelerates AML progression

We next assessed MSN gene mutations in human cancer samples derived from the TCGA (The Cancer Genome Atlas) and Catalog of Somatic Mutations in Cancer databases. This revealed MSN gene variants involving the R295 itself (H295 and S295) or in the RRRK-PDT motif (positions 293 to 299), a motif that has previously been suggested to be involved in human tumorigenesis (35). Specifically, cancers with such mutations included for endometrial carcinoma, melanoma, gastric adenocarcinoma, and large intestinal carcinomas and these variants (Fig. 4E, left) were all predicted to be deleterious, damaging, or pathogenic by Sorting Intolerant From Tolerant (SIFT) (36), PolyPhen (37), or Functional Analysis through Hidden Markov Models (FATHMM) (38). To functionally test whether these mutations might also associate with alterations in AML progression, we transplanted iMLL-ENL LICs retrovirally transduced with each of these variants into lethally irradiated recipients and assessed leukemia progression. This showed that S295 MSN expressing LICs succumbed to leukemia with kinetics very comparable to LICs with the aggressive/murine C295 variant (median latency, 25 days for S295 and 28 days for C295). Mice transplanted with H295 mutant MSN also displayed a pronounced shortening of disease development (median survival, 74 days as compared to 90 days for WT MSN). The disease progression from LICs with variants outside the R295 residue did not differ significantly from WT MSN. Together, these experiments revealed that variants that lead to alterations of the R295 residue of MSN seem to be particularly pathogenic, with a potential involvement of these MSN mutations as codrivers also in human cancer.

The R295C mutation modulates the structural dynamics and dimerization of moesin

The pathogenicity of the alterations at the R295 residue led us to next explore the structural effects of the C295 mutation. We first assessed the protein conformation of WT and C295 MSN using molecular dynamics simulation (MDS). This revealed that the β5C site at the 4.1 protein, ezrin, radixin, moesin (FERM) C-terminal domain of the WT protein was transformed to a random coil structure in C295 mutant MSN (Fig. 5A). This secondary structural element is highly conserved in MSN from different species as well as among other ERM proteins and has been previously suggested to be functionally important for MSN dimerization (39).

To try to functionally assess whether the C295 mutation affects MSN dimerization, we evaluated the WT or C295 mutant MSN dimer/monomer status in vivo using nondenaturing gel electrophoresis (Fig. 5B). This showed that C295 mutant MSN associated with a

decreased (approximately half) dimer formation and increased (approximately threefold) monomer formation compared to WT MSN (Fig. 5C). Together, these results suggested that the C295 mutation in MSN leads to structural changes in the protein that impair the ability of MSN to form self-inactivating homodimers.

Interactome analysis reveals minor alterations between WT and C295 mutant MSN

To explore potential changes in interactomes between WT and C295 mutant MSN, we next used mass spectrometry (MS) to identify proteins that bind to WT and C295 mutant MSN. WT and C295 mutant FLAG-tagged MSN–transduced LICs were subjected to FLAG immunoprecipitation followed by MS analysis, with empty vector–transduced LICs as a background control. By comparing the abundance of specific peptides between the background control and FLAG-tagged MSN samples, we identified 116 proteins enriched in the FLAG-tagged MSN samples (Fig. 5E and table S3). The identified interacting proteins included ezrin-radixin-moesin binding phosphoprotein-50 (EBP50), CD44 Antigen (CD44), Radixin (RDX), and Nucleoporin 93 (NUP93), which have previously been found to bind to ERM proteins (40). More generally, an interactome analysis revealed the interacting proteins to be enriched in biological pathways such as cytoskeleton cell movement, migration, and inflammation, which are all functionally relevant to previously attributed functions of MSN (Fig. 5D). However, no obvious alterations were detected when comparing the proteins bound to WT or C295 mutant MSN (Fig. 5E). Together, these results strongly suggested that the disease-promoting activities of C295 mutant MSN is not via a pronounced disruption of the ability to interact with other proteins.

C295 mutant MSN activates ERK signaling in a pMEK-independent manner

Alterations in the mitogen-activated protein kinase (MAPK)/extracellular signal–regulated kinase (ERK) pathway have frequently been implicated in leukemia (41), and the subclass of *MLL*r leukemia appears to have a particular propensity for activating mutations in this pathway (33, 42). Therefore, to test whether C295 mutant MSN dysregulates the MAPK/ERK pathway, we lastly assessed the ERK activity in WT or C295 mutant MSN–transduced LICs by Western blotting. This revealed that C295 mutant MSN associated with a significant increase of ERK phosphorylation compared to WT MSN [Fig. 6 (left and right, summary of data)], which in vivo extended to a persistent up-regulation of the ERK targets *Myc* and *Ccnd1* (Fig. 6, B and C).

To test whether the observed up-regulation of ERK phosphorylation associated with activation of MAPK kinase (MEK), we evaluated the activity of MEK. Somewhat unexpectedly, no increase of phosphorylated MEK (pMEK) was observed in C295 mutant MSN compared to WT MSN–transduced LICs. By contrast, a constitutively active RAS mutation (HRAS Q61L) resulted in significant increase in pERK and pMEK (Fig. 6). Together, these results established that leukemogenic activity of C295 mutant MSN, similar to the class of activating RAS mutations that are well established for *MLL*r AML, converges on enhanced ERK activity.

DISCUSSION

One way to gain insights into the stepwise processes in which normal cells become LICs is to build on the rich genetic information available from studies on human AML and explore such genetic circuits using relevant animal models. In the work described here,
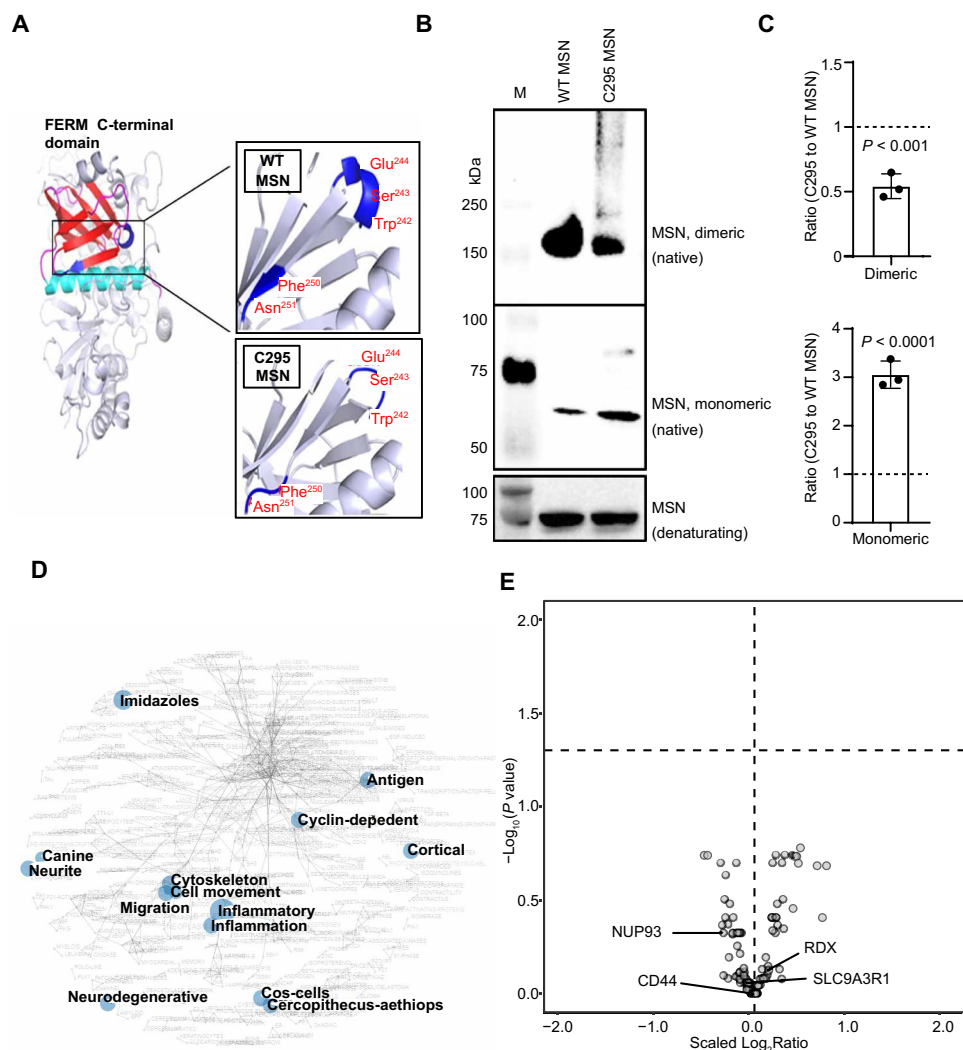
Fig. 5. The R295C mutation alters the structural dynamics of MSN, while the MSN interactomes is preserved in C295 mutant MSN. (**A**) Simulation of molecular dynamics of WT and C295 mutant MSN. Secondary structural changes at the FERM C-terminal domain of mutant MSN are shown in blue. In the C295 mutant structure, the highlighted region (composed of the amino acids Trp[242], Ser[243], Glu[244], Phe[250], and Asn[251]) has transformed from a β sheet and α helix to a random coil structure. (**B**) Nondenaturing gel electrophoresis of WT and C295 mutant MSN. Western blot with an anti-FLAG antibody was performed using nondenaturing (top) and denaturing (bottom) gel electrophoresis. (**C**) Densitometry profile showing the mean ratios ± SD of monomeric and dimeric MSN in cells transduced with WT or C295 mutant MSN in three independent experiments. (**D**) Enriched biological terms associated with MSN interactomes. (**E**) Volcano plot representation of abundance of interacting proteins of C295 mutant versus WT MSN from five biological replicates. The significance threshold ($P < 0.05$) is indicated with a dashed line at the y axis and fold change indicated at the x axis.

we explored an inducible model of MLL-ENL (*13*) with the aim of identifying secondary mechanisms that underlie transformation into overt AML. In the initial stages of our work, we established that clonality, a hallmark of human AML, is a key feature of AML also in the model used. Next, we set out to identify potential secondary mutations that could explain the disease pattern of MLL-ENL–associated AML.

Secondary somatic mutations have been reported in human AML in several studies (*31*, *43*), and the subclass of *MLL*r leukemia have a particular propensity for activating mutations in the RAS pathway (*33*, *42*). Furthermore, RAS-mutant clones are dominant at both AML progression and relapse (*33*, *42*). The molecular cross-talk between the activation of RAS/RAF/MAPK cascade and aberrant expression of *HOX* genes induced by MLL fusions appears to have a key role in the cooperative leukemogenesis of MLL fusions and *Ras*

mutations (*44*). Activating *Ras* mutations also have a strong impact in murine models of *MLL*r leukemia (*9*, *14*), although the degree to which these mutations arise spontaneously in murine models is less known. Among the somatic mutations identified in our work that could be unequivocally linked to the RAS pathway were activating mutations in *Hras*, *Ptpn11*, and *Braf*. These results further support the use of murine models to identify relevant biological pathways that underlie disease progression in human cells. Other mutations, including such affecting phosphatidylinositol 3-kinase–AKT, Janus kinase–signal transducers and activators of transcription, and receptor tyrosine kinase signaling pathways might also be relevant for AML progression, especially in the *Msn* WT cases (fig. S1).

A most prominent finding in our work was the identification and verification of a highly recurrent MSN R295C mutation upon
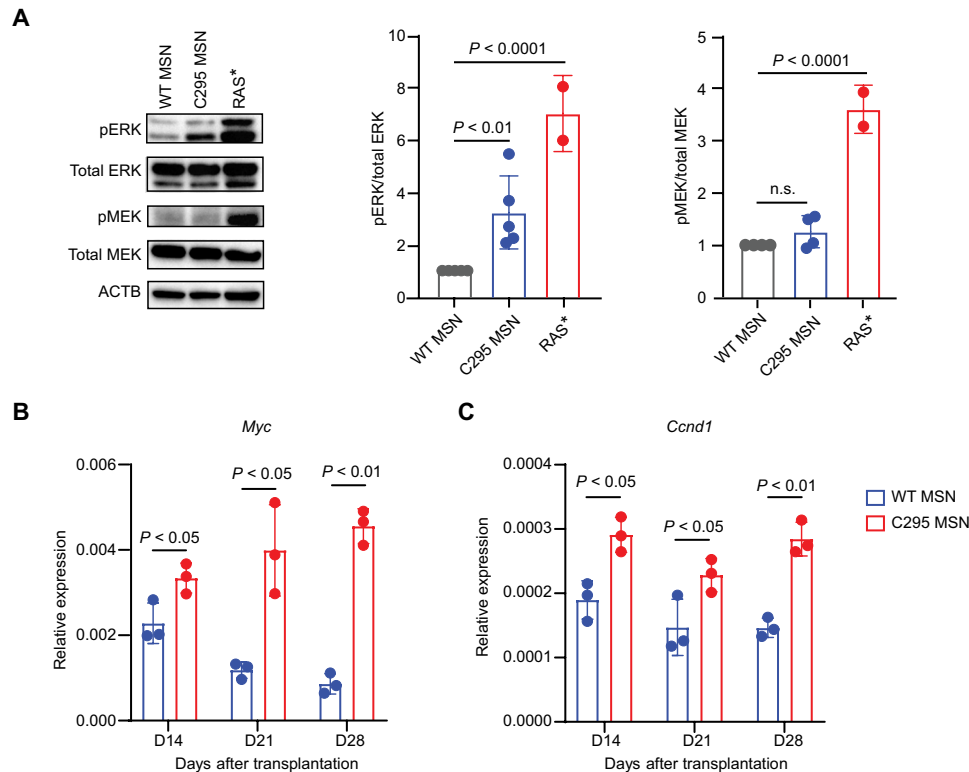
Fig. 6. C295 mutant MSN increases ERK phosphorylation in a pMEK-independent manner. (**A**) C295 mutant MSN increases ERK phosphorylation but not MEK phosphorylation. Left: Representative immunoblotting analysis showing the levels of pERK, pMEK, total ERK, and total MEK in WT ($n = 5$), C295 mutant MSN ($n = 5$), or HRAS L61 ($n = 2$) transduced LICs. β actin immunoblotting was used as loading control. Right: Summary of the ERK and MEK activity. Graphs show mean pERK/total ERK ± SD and mean pMEK/total MEK ± SD in two to five independent experiments. (**B** and **C**) mRNA expression of *Myc* and *Ccnd1* in GFP⁺ MLL-ENL in LICs with WT or C295 mutant MSN at different time points after transplantation. Data show means ± SD from three biological replicates (individual mice) per time point.

transformation. Surveying the literature, we observed that the MSN R295C mutation was previously identified in one case of a clathrin assembly lymphoid myeloid (CALM)/AF10 mouse model (*45*) and, more recently, as a recurrent somatic mutation in AML using a retroviral model of MLL-AF9 (*10*). In the work by Kotani *et al.* (*10*), it was proposed that the MSN R295C mutation is frequently "swept out" by other driver mutations in the process of clonal evolution of AML, perhaps suggesting the MSN R295C mutation to be more of a "passenger" than a "driver" mutation. This interpretation is not compatible with our results, which demonstrate that C295 mutant MSN plays a crucial role in both leukemia initiation and maintenance. Rather, we believe that the retroviral model system as used by Kotani *et al.* (*10*) might be characterized by a higher LIC polyclonality than the model system used here. Thereby, clonal competition eventually selects against MSN R295C mutant cells in favor of LICs carrying even more aggressive secondary mutations. Regardless, to our knowledge, no functional information on the consequence of the MSN R295C mutation on AML development has been provided previously.

MSN, a member of ERM family that also include ezrin and radixin, is best known for its involvement in regulating cell polarity, adhesion, and migration (*46*). In hematopoiesis, both MSN and ezrin are expressed, whereas radixin is mostly absent. MSN is the quantitatively dominant ERM protein in human blood cells and the only ERM family member expressed in platelets (*47*). However, neither expression levels nor mutations have to date been associated with

human AML (data from TCGA). Still, increasing evidence suggests that the dysregulation of cell signaling resulting from both altered MSN expression and its subcellular localization play crucial roles during progression of oral squamous cell carcinoma, melanoma, and breast cancer (*48–51*), and an MSN-anaplastic lymphoma kinase (ALK) fusion, resulting from a (X;2)(q11–12;p23) translocation, underlies the pathogenesis of anaplastic large cell lymphoma (*52*).

A germline R171W mutation leads to loss of MSN expression and associates with an X-linked immunodeficiency syndrome (*53*). Our results demonstrate that the R295C mutation is clearly different and relies on continuous MLL-ENL expression to propagate transformed cells. While it is well established that phosphorylation on the highly conserved T558 is associated with activation of MSN (*34*), we were somewhat puzzled that the phosphorylation on T558 impaired the transforming ability of the C295 mutant MSN. However, we note that a previous study observed that T558 phosphorylation of MSN in human myeloid cells led to diminished activation of the Rho guanosine triphosphatase CDC42 (*54*). This is likely of relevance also to *MLL*r AML, which relies on CDC42 activity to promote LIC self-renewal (*55*).

MSN contains a FERM domain with cloverleaf conformation of its F1, F2, and F3 subdomains (*56*). Notably, interactions mediated by the R295 residue in F3 and E87 in the F1 domain has been proposed to maintain the FERM domain stability (*56*). Disruption of interactions between F3 and F1, on the other hand, leads to F3

subdomain movements and destabilizes the FERM domain conformation (*56*). The F3 subdomain, which contains secondary structures including strand β5C (residues 245 to 251) and α1C helix (residues 274 to 297), is crucial for the function of MSN (*39*). The interaction between strand β5C and the FERM C-terminal residues (residues 295 to 304) was suggested to maintain homodimerization, an important mechanism for the stabilization and inactivation of MSN (*39*). Our protein simulation data provided support that the C295 mutation perturbs the secondary structures and stability of FERM domain in MSN. In addition, the R295C mutant MSN appears to exhibit a pronounced reduction in the amount of homodimers and increase in the amount of monomers, which further supported the notion of a disturbed FERM domain conformation in C295 mutant MSN. Notably and of relevance to MSN mutations found in human cancer, we observed that two mutations identified in human cancer, S295 and H295, also associated with pathogenicity in the murine MLL-ENL model. The correlation between the pathogenicity and the positive charge on the substituted residue supported that the mutation might function by perturbing the salt bridge interaction normally associated with R295. On the other hand, substitutions on residues R293 and R294 did not reveal any functional consequence for transformation, perhaps proposing a specific role for the substituted R295 residue.

While our proteomic data failed to reveal any apparent changes in the protein interactome as a consequence of the R295C mutation, we were able to establish induction of ERK signaling and its targets *Myc* and *Ccnd1* downstream of the mutation. This finding links previous observations, including mutations in *Braf*, *Ras*, and *Ptpn11*, as prominent secondary mutations in both human and murine *MLL*r AML models (*9*, *10*) and reinforces the promising prospect of ERK targeting in AML (*57*). While it seems that MSN mutant MLL-ENL–driven AML always associate to active ERK, we have observed instances of MLL-ENL AMLs with WT MSN in which ERK activation is less pronounced. Thus, while frequent, ERK activation might not be an absolute requirement for *MLL*r AML.

While further analysis will be required to explore how C295 mutant MSN stimulate the ERK signaling to accelerate AML progression, the ERM family protein ezrin was previously proposed to facilitate the encounter of RAS with its activating enzyme, thereby mediating spatiotemporal regulation of RAS activity (*58*, *59*). Our interactome analysis revealed direct binding between MSN and ERK. Therefore, C295 mutant MSN might affect ERK activity by regulating the encounter of ERK with its phosphorylating or dephosphorylating enzymes. Surveying the literature, we also noted that the RRRKPDT motif at residues 293 to 299, which is affected by the R295C mutation, has been implicated previously in propagation of human lung cancer via its direct regulation by a small RNA, piR-L-163 (*35*). R295 mutants might thereby function by altering the binding of small MSN regulatory RNAs, although how this would be connected to ERK activity is less clear.

We report here on the stepwise development of AML in a murine MLL-ENL model. Our study provides new insight into the evolutionary trajectories in murine *MLL*r AML, with the specific identification of a recurrent MSN R295C mutation and its function in leukemogenesis. We reveal a potential involvement of variants that lead to alterations of the R295 residue of MSN as codrivers also of human cancer. We believe that a better understanding of the biological roles and specific mechanisms of ERM proteins can be used for therapeutic benefit in human cancer, including AML.

MATERIALS AND METHODS

Mice
The generation and characterization of the iMLL-ENL model has been described previously (*13*). MLL-ENL expression was induced in vivo by administration of doxycycline in the food (2000 mg/kg; Ssniff Spezialdiäten GmbH). Eight to 12-week-old female C57BL/6N mice were used as recipients (Taconic; RRID: MGI:6196877), and iMLL-ENL mice were used at 8 to 14 weeks of age. Mice were maintained in the animal facilities at the Biomedical Center of Lund University, and all animal experiments were performed with the approval of a local ethics committee.

Evolution into AML from iMLL-ENL pGMs
A total of 5000 pGMs were isolated from iMLL-ENL mice (CD45.1⁺) using cell sorting (FACSAria II or III cell sorters; Becton Dickinson) and transplanted together with 300,000 unfractionated CD45.2⁺ BM cells into lethally irradiated (900 rads) CD45.2⁺ mice. Recipients were put on a doxycycline-containing diet 5 days before transplantation to ensure expression of MLL-ENL immediately after transplantation.

Assessment of clonality of developing leukemias
A lentiviral guide RNA (gRNA) library containing 87,897 individual gRNA sequences was repurposed here for cellular barcoding. The genome-wide mouse lentiviral CRISPR gRNA library was a gift from K. Yusa (Addgene, no. 50947) (*19*). For the lentivirus production, 3 μg of a lentiviral vector, 9 μg of ViraPower Lentiviral Packaging Mix (Invitrogen), and 12 μl of PLUS Reagent were added to 3 ml of Opti-MEM and incubated for 5 min at room temperature. Thirty-six microliters of the LTX reagent was then added to this mixture and further incubated for 30 min at room temperature. The transfection complex was added to 80% confluent human embryonic kidney 293-FT (American Type Culture Collection, PTA-5077; RRID: CVCL_6911) cells in a 10-cm dish and incubated for 3 hours. The medium was replaced with fresh medium 24 hours after transfection (*19*). Viral supernatant was harvested 48 hours after transfection and stored at −80°C. pGMs from iMLL-ENL mice were isolated and transduced with lentivirus by centrifugation of the lentivirus (2 hours, 1200*g*, and 32°C) over RetroNectin (Takara Bio)–coated plates according to the manufacturer's instructions and coculture of the cells over the virus-coated wells overnight at 37°C. Transduction rates were aimed <30% to minimize the risk of infection of individual cells with multiple barcodes. Forty-eight hours after transduction, 5000 transduced cells [blue fluorescent protein (BFP)] were sorted and transplanted into lethally irradiated (900 rads) WT recipients (CD45.2⁺) together with 300,000 unfractionated BM cells (CD45.2⁺). At leukemic transformation, gDNA was purified from individual leukemic recipient BM cells using the PureLink Genomic DNA Isolation Kit (Thermo Fisher Scientific) and the 20–base pair (bp) barcodes were amplified by PCR. Barcodes were amplified using Q5 High-Fidelity DNA Polymerase (New England Biolabs) with the following cycling conditions: 30 s at 98°C, 32 cycles of 10 s at 98°C, 30 s at 65°C, and 30 s at 72°C, followed by a final 2-min extension at 72°C. Primers used were ACGATACAAGGCTGTTAGAGAGA (forward) and CGGTGCCACTTTTTCAAGTT (reverse). Following PCR, Sanger sequencing of the barcodes was performed (Eurofins).

Retroviral production and transduction
An *Msn* cDNA was cloned using Gibson assembly (New England Biolabs) into an Eco RI and Xho I linearized MigR1 retroviral vector

(60) to generate the *Msn*-WT–green fluorescent protein (GFP) construct. Other *Msn* variants vectors were generated by using a Q5 Site-Directed Mutagenesis kit (New England Biolabs) from the *Msn*-WT constructs. An shRNA targeting *Msn* were selected from a mouse genome-wide sensor-based shRNA predictions library and cloned into the retroviral-based shRNA expression vector LENG, as previously described (61). LENG was a gift from J. Zuber (Addgene, plasmid no. 111162). Replication-incompetent retroviruses were produced by transfecting the vectors into Plat-E packaging cells (RRID: CVCL_B488) using Lipofectamine LTX Reagent with PLUS Reagent (Thermo Fisher Scientific). Virus-containing supernatants were harvested 48 hours after transfection. Retroviral transductions were performed by centrifugation of the retrovirus (2 hours, 1200*g*, and 32°C) over RetroNectin (Takara Bio)–coated plates according to the manufacturer's instructions and coculture of the cells over the virus-coated wells for 48 hours at 37°C.

Transduction and transplantation of LICs

To assess the role of C295 MSN in normal hematopoiesis, we transduced BM LSK (Lin⁻Sca1⁺cKit⁺) cells from WT C57BL/6 mice (CD45.2⁺) with either WT or R295C mutant MSN containing retrovirus. Cells were cultured in StemSpan serum-free expansion media (STEMCELL Technologies) supplemented with gentamicin (50 ng/ml; Invitrogen), 100 μM 2-mercaptoethanol (Thermo Fisher Scientific), mouse Interleukin-3 (mIL-3) (5 ng/ml), human Flt3-Ligand (hFlt3) (20 ng/ml), mouse thrombopoietin (mTPO) (10 ng/ml), mouse stem cell factor (mSCF) (50 ng/ml; all from PeproTech), and doxycycline (1 μg/ml; Sigma-Aldrich).

Forty-eight hours after transduction, 2000 donor cells were competitively transplanted into lethally irradiated WT recipient hosts (CD45.1⁺) together with 300,000 unfractionated CD45.1⁺ BM cells per mouse. At the experimental end point (28 weeks after transplantation), reconstitution was assessed by FACS analysis of PB. To assess the influence of MSN variants for *MLL*-ENL leukemia progression, GMLPs and pGMs (LICs) were isolated as described previously (13) from iMLL-ENL mice and transduced with retroviruses expressing WT, C295, A558, D558, C295 + D558, or C295 + A558 MSN. Forty-eight hours after transduction, 6000 GFP⁺ transduced cells were sorted and transplanted into lethally irradiated (900 rads) WT recipients (CD45.2⁺) together with 300,000 unfractionated BM. To assess the influence of MSN for MLL-ENL leukemia progression, GMLPs and pGMs (LICs) were transduced with retroviruses expressing a scramble or *Msn*-targeting shRNA. Following transduction, 3000 GFP⁺ transduced cells were sorted and transplanted into lethally irradiated (900 rads) WT recipients (CD45.2⁺) together with 300,000 unfractionated BM cells to ensure survival of transplanted hosts. To assess the leukemogenic activity of MSN variants H295, S295, C294, and C293 identified in human cancers, we transplanted 6000 transduced iMLL-ENL LICs per mouse into lethally irradiated (900 rads) WT recipients (CD45.2⁺) together with 300,000 unfractionated BM. For secondary transplantations, leukemic blasts were collected from primary AML samples with the C295 mutant MSN. For evaluation of MLL-ENL dependence, 100,000 candidate AML cells were transplanted to secondary recipients with or without MLL-ENL induction. For evaluation of the impact of the C295 MSN on AML propagation, primary AML cells were transduced with retroviruses expressing *Msn* shRNA or scramble shRNA. Forty-eight hours after transduction, 100,000 GFP⁺ leukemic blasts were sorted and transplanted into sublethally irradiated (450 rad)

WT recipients (CD45.2⁺). Where relevant, recipients were put on a doxycycline-containing diet 5 days before transplantation to ensure continuous expression of MLL-ENL. Survival rates were plotted using the Kaplan-Meier method (GraphPad Prism). Mortality, rapid elevations in donor myeloid chimerism, and signs of morbidity according to ethical guidelines were considered events for plotting event-free survival. Cells were sorted on a FACSAria II or III cell sorter (Becton Dickinson). The following antibodies were used for flow cytometry: anti-mouse CD117 (c-Kit)-APC (BioLegend, catalog no. 105812; RRID: AB_1282964), anti-mouse/human B220 Biotin (BioLegend, catalog no. 103203; RRID: AB_312988), anti-mouse CD4-Biotin (SONY, catalog no. 1102020; RRID: AB_1848918), anti-mouse CD8-Biotin (SONY, catalog no. 1103520; RRID: AB_962670), anti-mouse Ly-6G/Ly-6C (Gr-1)-Biotin (BioLegend, catalog no. 108404; RRID: AB_313369), anti-mouse TER-119-Biotin (BioLegend, catalog no. 116203; RRID: AB_313704), SAv-Brilliant Violet 605 (SONY, catalog no. 2626145), anti-mouse Ly-6A/E (Sca-1)–Pacific Blue (BioLegend, catalog no. 122520; clone E13-161.7), anti-mouse CD48–fluorescein isothiocyanate (FITC; BioLegend, catalog no. 103404; RRID: AB_313018), anti-mouse CD150-PE (BioLegend, catalog no. 115904; RRID: AB_313683), anti-mouse CD105-PE-Cy7 (Thermo Fisher Scientific, catalog no. 25-1051-82; RRID: AB_2573379), anti-mouse CD16/CD32–Alexa Fluor 700 (Thermo Fisher Scientific, catalog no. 56-0161-82; RRID: AB_493994), anti-mouse CD36-APC (BioLegend, catalog no. 102612; RRID: AB_2072639), anti-mouse Gr-1–Brilliant Violet 711 (SONY, catalog no. 1142215; clone RB6-8C5), anti-mouse CD127 (IL7Ra)-FITC (Thermo Fisher Scientific, catalog no. 11-1271-85; RRID: AB_465196), and anti-mouse CD135 (Flt3)-PE (Thermo Fisher Scientific, catalog no. 12-1351-83; RRID: AB_465860) All flow cytometry and FACS data were analyzed using FlowJo software (version 10.3, Tree Star).

Phenotypic analyses of the AML development

Diseased mice were subjected to automated blood counting (Sysmex KX-21N) analyses. Morphological analysis of GFP⁺ BM cells were spun on a glass slide using a Shandon Cytospin (Thermo Scientific) and air-dried. Slides were stained for 5 min in May-Grünwald staining solution (Sigma-Aldrich), washed for 5 min in phosphate-buffered saline, and stained for 17 min in Giemsa stain (Sigma-Aldrich) diluted 1:20 in deionized water. Slides were rinsed in deionized water, air-dried, and visualized under a Nikon TE2000-S microscope. For each sample, four to five images were taken by a QImaging camera and QCapture Pro software (Fryer Company Inc.). Two hundred cells from each sample were evaluated to quantify blasts and differentiated cells.

Whole-genome and whole-exome sequencing

gDNA was extracted from donor and recipient BM with the PureLink Genomic DNA Kit (Invitrogen) for whole-genome sequencing (WGS) or whole-exome sequencing (WES). WES (Agilent SureSelect whole exome capture 50 Mb, mouse) was performed on nine independent leukemia derived from different types of LICs and two additional donor-recipient pairs (cohort pGM_3 and pGM_4). In addition, we subjected 10 independent leukemias from a non–transplantation-based MLL-ENL model (32) to WES. WGS was performed on one donor-recipient pair (cohort pGM_2), but analysis was restricted to exonic regions. Samples were sequenced using Illumina instruments. Raw reads were checked for quality with FastQC (v.0.11.2) (62) and mapped to mouse reference genome GRCm38 using BWA mem (v. 0.7.10) (63). Duplicated reads were removed with SAMtools (v. 0.1.19) (64). Mapped reads were further realigned, and bases

were recalibrated with genome analysis toolkit GATK using known variants from C57BL/6NJ, 129S1/SvImJ for the detection of single-nucleotide variations (SNVs), insertions and deletions (indel), and copy number variations/alterations (65). All functional annotations were based on ENSEMBL genes. SNV and indel calling were performed on a donor–single recipient basis using GATK MuTect2 (65). SNVs and indels detected by the above software were subsequently filtered by a homemade pipeline, (i) excluding all the reported mutations with low depth (allele depth, <15); (ii) selecting the protein coding mutations; (iii) selecting the missense and frameshift mutations; (iv) excluding mutations with low allele frequency (allele frequency, <0.1); (v) excluding germline mutations detected from reference samples in cohorts pGM_2, pGM_3, and pGM_4; (vi) excluding common single-nucleotide polymorphisms reported in mouse strains mgp.v4-C57BL/6NJ-129S1/SvImJ-129S5SvEvBrd and PROVEAN (66). (vii) All the somatic missense mutations were annotated by SnpEff, and their functional consequences were evaluated using PROVEAN (66) and SIFT (36). FASTQ files were deposited at the Sequence Read Archive (SRA) with the dataset identifier PRJNA799845.

Ultradeep targeted sequencing
gDNA was extracted from female uninduced iMLL-ENL and WT C57BL/6 ckit$^+$ cells. Six hundred nanograms of gDNA from ~100,000 cells (200,000 alleles) was used to generate the sequencing libraries for each sample. For the synthesized WT and MUT *Msn* oligo controls, an input estimated to contain 200,000 copies was used. Amplicons of ~180 bp containing the region of interest were amplified using PCR with custom primers. The amplified PCR products were cleaned up using SPRIselect beads (Beckman Coulter). A second PCR was then performed to add index and sequencing adapters. The amplified final libraries were cleaned up using SPRIselect beads (Beckman Coulter). Purified libraries were run on Agilent High Sensitivity DNA Kit chip (Agilent Technologies) to verify desired size distribution, quantified by Qubit dsDNA HS Assay Kit (Thermo Fisher Scientific), and pooled at equimolar concentrations. Pooled libraries were loaded on an Illumina MiSeq Reagent Nano Kit v2 flow cell following protocols for single-end 50-cycle sequencing. Sequencing data were downloaded as FASTQ files that were further assessed with the quality control tool FastQC (v.0.11.2) (62), including read count, base quality across reads, and guanine and cytosine (GC) content per sequence. Reads were evaluated at the c.833 position for base calls supporting the c.833C>T mutation.

Protein structure prediction and simulation of molecular dynamics
The three-dimensional structures of the WT and mutant moesin were determined using the comparative modeling approach Modeller 9.214 (67). For target-template alignment, we used three known template structures (Protein Data Bank IDs: 1e5wA, 5j0kA, and 2i1jA). The modeled structures were evaluated on the basis of the template structures using RAMPAGE (68). MDS was performed using the GROMACS 4.6.3 package. GROMOS96 43a1 force field was used for all MDS (69). Before performing MDS, water molecules were removed and the structures were solvated in cubic of simple point charge water molecules and periodic boundary conditions. The topology files were generated by GROMOS force field; then, the steepest descent method was applied for energy minimization. Before starting dynamics, five chlorine molecules were added to neutralize the system. Equilibration of the system was kept at a constant temperature of 300 K. The equilibrated systems were then subjected to MDS for 100 ns. For every 5 ns, the trajectory files were saved for further analysis.

Western blot analysis
Native (nondenaturing) conditions
FLAG-tagged sequences [3x FLAG(DYKDDDDK)] were cloned into the WT and C295 MSN at the C terminus by using Q5 Site-Directed Mutagenesis (New England Biolabs). WT-MSN-3xFLAG and C295-MSN-3xFLAG retroviruses were produced and transduced into NIH 3T3 (CLS, catalog no. 400101/p677_NIH-3T3; RRID: CVCL_0594) cells. Two days after the transduction, transduced cells were isolated and expanded in vitro for five more days. A total of 10^7 cells were lysed in 1 ml of ice-cold radioimmunoprecipitation assay lysis buffer [150 mM NaCl, 1% NP-40, 0.5% sodium-deoxycholate, 0.1% SDS, and 10 mM tris-HCl (pH 8)] supplemented with a protease inhibitor cocktail (Roche). Lysates were cleared by centrifugation at 15,000 rpm for 15 min at 4°C, and supernatants were removed and assayed for protein concentration using the Quick Start Bradford Protein Assay Kit (Bio-Rad). Each sample was aliquoted into two parts. One aliquot was mixed with Novex Tris-Glycine Native Sample Buffer (2×) (Thermo Fisher Scientific) without denaturation, and equal amounts of protein from WT and C295 mutant MSN samples were subjected to 4 to 20% Tris-Glycine Gels (Invitrogen) and transferred to polyvinylidene difluoride membranes (Bio-Rad). The other aliquot was denatured by mixing with an appropriate amount of NuPAGE LDS Sample Buffer (4×) (Thermo Fisher Scientific) containing 2.5% 2-mercaptoethanol and boiling at 95°C for 5 min. Equal amounts of proteins from WT and C295 mutant MSN samples were subjected to SDS–polyacrylamide gel electrophoresis as reference for total input levels of the FLAG-tagged proteins. The 3xFLAG-Tag was detected with a rabbit anti-FLAG antibody (1:1000; Invitrogen, PA1-984B; RRID: AB_347227). Horseradish peroxidase–conjugated donkey anti-rabbit immunoglobulin G (1:5000; GE Healthcare, NA934) was used as the secondary antibody. The antibody-labeled proteins were illuminated with SuperSignal West Femto Maximum Sensitivity Substrate (Thermo Fisher Scientific) and exposed to imaging films on the ChemiDoc MP Imaging System (Bio-Rad).

Denaturing conditions
For determination of MAPK signaling, iMLL-ENL LICs were isolated and transduced with WT, C295 mutant MSN, or L61 HRAS. Two days after transduction, transduced cells were sorted and grown in vitro for 5 more days. A total of 10^7 cells were lysed, cleared, and further processed as above. The following antibodies were used: rabbit β-actin (1:1000; Cell Signaling Technology, 4970; RRID: AB_2223172), rabbit p44/42 MAPK (Erk1/2) (1:1000; Cell Signaling Technology, 9102; RRID: AB_330744), rabbit phospho-p44/42 MAPK (Erk1/2) (Thr^{202}/Tyr^{204}) (1:1000; Cell Signaling Technology, 9101), rabbit MEK1/2 (1:1000; Cell Signaling Technology, 9122; RRID: AB_823567), and rabbit phospho-MEK1/2(Ser$^{217/221}$) (1:1000; Cell Signaling Technology, 9121). For determination of MSN protein level upon *Msn* shRNA knockdown, iMLL-ENL LICs were isolated and transduced with scramble or *Msn* shRNA. Two days after transduction, transduced cells were collected, lysed, and processed as above. Rabbit moesin (1:1000; Abcam, ab52490; RRID: AB_881245) was used.

Immunoprecipitation and MS
Sample preparation for protein mass spectroscopy
WT-MSN-3xFLAG, C295-MSN-3xFLAG, or empty MigR1 vector retrovirus–transduced iMLL-ENL LICs (five biological replicates/individual

mice were included per group) were lysed in 1 ml of ice-cold immuno-precipitation buffer [50 mM tris-HCl (pH 7.4), 150 mM NaCl, 1% NP-40, and protease inhibitor]. Lysates were cleared by centrif-ugation at 15,000 rpm for 15 min at 4°C, and supernatants were re-moved and assayed for protein concentration using the Quick Start Bradford Protein Assay Kit (Bio-Rad). Equal amounts of proteins from WT, C295 mutant MSN, or empty vector–transduced LICs were incubated with 40 μl of Anti-FLAG M2 Magnetic Beads (Sigma-Aldrich, M8823; RRID: AB_2637089) for 6 hours in the cold and then washed six times in immunoprecipitation wash buffer [50 mM tris-HCl (pH 7.4), 150 mM NaCl, 0.3% NP-40, and protease inhibitor]. Beads bound with FLAG-tagged proteins were then washed with 200 mM Hepes, and bound proteins were digested on beads with trypsin (5 μg/ml) in 200 mM Hepes/0.1% RapiGest for 7 hours at 37°C. Supernatant containing peptides was collected, and proteins remaining on beads were further digested with trypsin (5 μg/ml) in 200 mM Hepes/0.1% RapiGest/1 mM dithiothreitol for 1.5 hours at 37°C. Supernatant was collected, and both supernatants were com-bined. Digested peptide mixtures were desalted and purified using Oasis HLB cartridges (Waters). Columns were primed and condi-tioned in three steps using pure methanol, 80% acetonitrile (ACN), and 0.1% formic acid (FA) in ultrapure water and 0.1% FA in water, respectively. Samples were loaded on columns, and eluates were loaded again to maximize recovery. Columns were washed four times with 0.1% FA in water, and peptides were subsequently eluted in 45% ACN and 0.1% FA in water. Eluates were dried and stored at −80°C before MS analysis.

MS analysis
Before MS analysis, purified peptide mixtures were reconstituted with 3% ACN and 0.1% FA in ultrapure water, and peptide concen-tration was measured on a DS-11-FX (DeNovix) at 215 nm. Global proteome MS analysis was performed on a Q-Exactive HF-X (Thermo Fisher Scientific) MS. The volume equivalent of 1 μg of tryptic pep-tides from each sample was trapped on an Acclaim PepMap 100 precolumn (ID, 75 μm by 2 cm; C18, 3 μm; 100 Å resin; Thermo Fisher Scientific) and then separated on a reverse-phase EASY-Spray HPLC column (ID, 75 μm by 50 cm; C18, 2 μm; 100 Å resin; Thermo Fisher Scientific) coupled to a Proxeon nano–liquid chromatography EASY 1200 system (Thermo Fisher Scientific). Peptides were eluted in a 120-min gradient (flow, 350 nl/min; mobile phase A, 0.1% FA in H_2O; mobile phase B, 80% ACN and 0.1% FS). Gradient was as follows: 10 to 30% B in 90 min, 30 to 45% B in 20 min, 45 to 95% B in 0.5 min, and 95% B for 9 min. Full MS scan parameters were as follows: 60,000 resolution and AGC target was set to 3E6. Tandem MS scan parameters were as follows: 15,000 resolution and AGC target was set to 1E5. Collision energy was set to 28, and n of ana-lyzed peaks was set to 15. Dynamic exclusion window was set to 10 s.

MS data processing
MS files were analyzed using MaxQuant (70) (v1.6.3.4), and MS spectra searched using the Andromeda (71) search engine with the UniProt–Swiss-Prot mouse proteome database (version download, 2021.02.08; selected enzyme, trypsin). Carbamidomethylation of Cys residues was selected as fixed modification, while Met oxidation and acetylation of N-terminal residues were selected as variable ones. Label-free quantification (LFQ) was activated for the proteome data search. Identification of peptides resulting from missed cleavages was allowed. Precursor ion tolerances were 20 and 4.5 parts per million for first and main searches, respectively. Match-between-run option was enabled, and settings were left to default. Protein LFQ intensities

were used for downstream proteome analyses. The protein abundance table were filtered for protein q value (cutoff, 0.01), contaminant (excluded), reverse sequences (excluded), unique peptides (at least 1).

Data analysis
LFQ intensities were $\log_2$-transformed and filtered to select high-confidence interactors by using Welch corrected t test (P value cutoff, 0.05) and quantitative enrichment measure ($\log_2$ ratio to negative con-trol; >0). WT and mutant samples were filtered separately against the empty MigR1 vector control. Missing data were then applied (four of five observations needed). The filtered dataset was subsequently cen-tered and scaled. Statistical differences between WT and mutant models were assessed by Welch t test (Benjamini-Hochberg adjusted P value cutoff, 0.05). Analyses were performed in GraphPad (v9.0) and R (v3.6).

Data accession
MS files have been deposited to the ProteomeXchange Consortium via the PRIDE partner repository with the dataset identifier PXD028261.

qRT-PCR
Total RNA was isolated using a single-cell RNA purification kit (Norgen Biotek) and converted to cDNA using SuperScript III First-Strand Synthesis System (Invitrogen). qRT-PCR reactions were run with SYBR GreenER (Invitrogen) on a CFX96 Touch Real-Time PCR Detection System (Bio-Rad). All signals were quantified using the ΔCt method and were normalized to β-actin mRNA expression levels.

Statistical analysis
Data analysis was performed using Microsoft Excel and GraphPad Prism (GraphPad Software). All FACS data were analyzed with FlowJo (Tree Star). Significance values were calculated by Student's two-tailed t test or the log rank test (Mantel-Cox test) for Kaplan-Meier curves.

SUPPLEMENTARY MATERIALS
Supplementary material for this article is available at https://science.org/doi/10.1126/sciadv.abm9987

View/request a protocol for this paper from *Bio-protocol*.

REFERENCES AND NOTES
1. R. L. Bowman, L. Busque, R. L. Levine, Clonal hematopoiesis and evolution to hematopoietic malignancies. *Cell Stem Cell* **22**, 157–170 (2018).
2. J. C. Wang, J. E. Dick, Cancer stem cells: Lessons from leukemia. *Trends Cell Biol.* **15**, 494–501 (2005).
3. K. Mitchell, U. Steidl, Targeting immunophenotypic markers on leukemic stem cells: How lessons from current approaches and advances in the leukemia stem cell (LSC) model can inform better strategies for treating acute myeloid leukemia (AML). *Cold Spring Harb. Perspect. Med.* **10**, a036251 (2020).
4. A. V. Krivtsov, S. A. Armstrong, MLL translocations, histone modifications and leukaemia stem-cell development. *Nat. Rev. Cancer* **7**, 823–833 (2007).
5. V. Grossmann, S. Schnittger, F. Poetzinger, A. Kohlmann, A. Stiel, C. Eder, A. Fasan, W. Kern, T. Haferlach, C. Haferlach, High incidence of RAS signalling pathway mutations in MLL-rearranged acute myeloid leukemia. *Leukemia* **27**, 1933–1936 (2013).
6. E. Papaemmanuil, M. Gerstung, L. Bullinger, V. I. Gaidzik, P. Paschka, N. D. Roberts, N. E. Potter, M. Heuser, F. Thol, N. Bolli, G. Gundem, P. van Loo, I. Martincorena, P. Ganly, L. Mudie, S. McLaren, S. O'Meara, K. Raine, D. R. Jones, J. W. Teague, A. P. Butler, M. F. Greaves, A. Ganser, K. Döhner, R. F. Schlenk, H. Döhner, P. J. Campbell, Genomic classification and prognosis in acute myeloid leukemia. *N. Engl. J. Med.* **374**, 2209–2221 (2016).
7. A. K. Andersson, J. Ma, J. Wang, X. Chen, A. L. Gedman, J. Dang, J. Nakitandwe, L. Holmfeldt, M. Parker, J. Easton, R. Huether, R. Kriwacki, M. Rusch, G. Wu, Y. Li, H. Mulder, S. Raimondi, S. Pounds, G. Kang, L. Shi, J. Becksfort, P. Gupta, D. Payne-Turner, B. Vadodaria, K. Boggs, D. Yergeau, J. Manne, G. Song, M. Edmonson, P. Nagahawatte, L. Wei, C. Cheng, D. Pei, R. Sutton, N. C. Venn, A. Chetcuti, A. Rush, D. Catchpoole, J. Heldrup, T. Fioretos, C. Lu, L. Ding, C.-H. Pui, S. Shurtleff, C. G. Mullighan, E. R. Mardis, R. K. Wilson, T. A. Gruber, J. Zhang, J. R. Downing; St. Jude Children's Research

Hospital–Washington University Pediatric Cancer Genome Project, The landscape of somatic mutations in infant *MLL*-rearranged acute lymphoblastic leukemias. *Nat. Genet.* **47**, 330–337 (2015).

8. T. A. Milne, Mouse models of MLL leukemia: Recapitulating the human disease. *Blood* **129**, 2217–2223 (2017).

9. A. Hyrenius-Wittsten, M. Pilheden, H. Sturesson, J. Hansson, M. P. Walsh, G. Song, J. U. Kazi, J. Liu, R. Ramakrishan, C. Garcia-Ruiz, S. Nance, P. Gupta, J. Zhang, L. Rönnstrand, A. Hultquist, J. R. Downing, K. Lindkvist-Petersson, K. Paulsson, M. Järås, T. A. Gruber, J. Ma, A. K. Hagström-Andersson, De novo activating mutations drive clonal evolution and enhance clonal fitness in KMT2A-rearranged leukemia. *Nat. Commun.* **9**, 1770 (2018).

10. S. Kotani, A. Yoda, A. Kon, K. Kataoka, Y. Ochi, Y. Shiozawa, C. Hirsch, J. Takeda, H. Ueno, T. Yoshizato, K. Yoshida, M. M. Nakagawa, Y. Nannya, N. Kakiuchi, T. Yamauchi, K. Aoki, Y. Shiraishi, S. Miyano, T. Maeda, J. P. Maciejewski, A. Takaori-Kondo, S. Ogawa, H. Makishima, Molecular pathogenesis of disease progression in MLL-rearranged AML. *Leukemia* **33**, 612–624 (2019).

11. L. Chen, W. Chen, J. Mysliwski, J. Serio, J. Ropa, F. A. Abulwerdi, R. J. Chan, J. P. Patel, M. S. Tallman, E. Paietta, A. Melnick, R. L. Levine, O. Abdel-Wahab, Z. Nikolovska-Coleska, A. G. Muntean, Mutated Ptpn11 alters leukemic stem cell frequency and reduces the sensitivity of acute myeloid leukemia cells to Mcl1 inhibition. *Leukemia* **29**, 1290–1300 (2015).

12. D. H. Christiansen, M. K. Andersen, F. Desta, J. Pedersen-Bjergaard, Mutations of genes in the receptor tyrosine kinase (RTK)/RAS-BRAF signal transduction pathway in therapy-related myelodysplasia and acute myeloid leukemia. *Leukemia* **19**, 2232–2240 (2005).

13. A. Ugale, G. L. Norddahl, M. Wahlestedt, P. Säwén, P. Jaako, C. J. Pronk, S. Soneji, J. Cammenga, D. Bryder, Hematopoietic stem cells are intrinsically protected against MLL-ENL-mediated transformation. *Cell Rep.* **9**, 1246–1255 (2014).

14. A. Ugale, P. Säwén, M. Dudenhöffer-Pfeifer, M. Wahlestedt, G. L. Norddahl, D. Bryder, MLL-ENL-mediated leukemia initiation at the interface of lymphoid commitment. *Oncogene* **36**, 3207–3212 (2017).

15. C. J. Pronk, D. J. Rossi, R. Månsson, J. L. Attema, G. L. Norddahl, C. K. F. Chan, M. Sigvardsson, I. L. Weissman, D. Bryder, Elucidation of the phenotypic, functional, and molecular topography of a myeloerythroid progenitor cell hierarchy. *Cell Stem Cell* **1**, 428–442 (2007).

16. S. C. Kogan, J. M. Ward, M. R. Anver, J. J. Berman, C. Brayton, R. D. Cardiff, J. S. Carter, S. de Coronado, J. R. Downing, T. N. Fredrickson, D. C. Haines, A. W. Harris, N. L. Harris, H. Hiai, E. S. Jaffe, I. MacLennan, P. P. Pandolfi, P. K. Pattengale, A. S. Perkins, R. M. Simpson, M. S. Tuttle, J. F. Wong, H. C. Morse III; Hematopathology subcommittee of the Mouse Models of Human Cancers Consortium, Bethesda proposals for classification of nonlymphoid hematopoietic neoplasms in mice. *Blood* **100**, 238–245 (2002).

17. T. Velasco-Hernandez, A. Hyrenius-Wittsten, M. Rehn, D. Bryder, J. Cammenga, HIF-1α can act as a tumor suppressor gene in murine acute myeloid leukemia. *Blood* **124**, 3597–3607 (2014).

18. M. Almosailleakh, J. Schwaller, Murine models of acute myeloid leukaemia. *Int. J. Mol. Sci.* **20**, 453 (2019).

19. H. Koike-Yusa, Y. Li, E. P. Tan, C. Velasco-Herrera Mdel, K. Yusa, Genome-wide recessive genetic screening in mammalian cells with a lentiviral CRISPR-guide RNA library. *Nat. Biotechnol.* **32**, 267–273 (2014).

20. H. G. V. Einsiedel, T. Taube, B. Beyermann, S. Dragon, A. Möricke, C. Kebelmann-betzig, J. Köchling, G. Ü. N. Henze, K. Seeger, Absence of mutations in the CDKN2 binding site of CDK4 in childhood acute lymphoblastic leukemia. *Leuk. Lymphoma* **40**, 413–417 (2001).

21. M. Yilmaz, F. Wang, S. Loghavi, C. Bueso-Ramos, C. Gumbs, L. Little, X. Song, J. Zhang, T. Kadia, G. Borthakur, E. Jabbour, N. Pemmaraju, N. Short, G. Garcia-Manero, Z. Estrov, H. Kantarjian, A. Futreal, K. Takahashi, F. Ravandi, Late relapse in acute myeloid leukemia (AML): Clonal evolution or therapy-related leukemia? *Blood Cancer J.* **9**, 1–6 (2019).

22. M. Ojeda-Uribe, E. Jeandidier, P. Cornillet-Lefebvre, A. Le Bechec, L. Mauvieux, Molecular profiling by whole-exome-sequencing of two patients with t-AML post combined therapy of acute promyelocytic leukemia. *Exp. Hematol.* **53**, S74 (2017).

23. M. Garg, Y. Nagata, D. Kanojia, A. Mayakonda, K. Yoshida, S. Haridas Keloth, Z. J. Zang, Y. Okuno, Y. Shiraishi, K. Chiba, H. Tanaka, S. Miyano, L. W. Ding, T. Alpermann, Q. Y. Sun, D. C. Lin, W. Chien, V. Madan, L. Z. Liu, K. T. Tan, A. Sampath, S. Venkatesan, K. Inokuchi, S. Wakita, H. Yamaguchi, W. J. Chng, S. K. Y. Kham, A. E. J. Yeoh, M. Sanada, J. Schiller, K. A. Kreuzer, S. M. Kornblau, H. M. Kantarjian, T. Haferlach, M. Lill, M. C. Kuo, L. Y. Shih, I. W. Blau, O. Blau, H. Yang, S. Ogawa, H. P. Koeffler, Profiling of somatic mutations in acute myeloid leukemia with *FLT3*-ITD at diagnosis and relapse. *Blood* **126**, 2491–2501 (2015).

24. J. Takeda, K. Yoshida, M. M. Nakagawa, Y. Nannya, A. Yoda, D. Morishita, R. Saiki, K. Chiba, H. Tanaka, Y. Shiraishi, M. C. Kuo, C. M. Kerr, Y. Nagata, N. Hiramoto, A. Hangaishi, H. Nakazawa, K. Ishiyama, S. Miyano, S. Chiba, Y. Miyazaki, T. Kitano, N. Usuki, N. Sezaki, H. Tsurumi, S. Miyawaki, J. P. Maciejewski, T. Ishikawa, K. Ohyashiki, A. Ganser, M. Heuser, F. Thol, L. Y. Shih, A. Takaori-Kondo, H. Makishima, S. Ogawa, EPOR/JAK/STAT signaling pathway as therapeutic target of acute erythroid leukemia. *Blood* **138**, 610 (2021).

25. P. Prasad, A. Lennartsson, K. Ekwall, The roles of SNF2/SWI2 nucleosome remodeling enzymes in blood cell differentiation and leukemia. *Biomed. Res. Int.* **2015**, 347571 (2015).

26. L. Shih, D.-C. Liang, C.-F. Huang, Y.-T. Chang, C.-L. Lai, T.-H. Lin, C.-P. Yang, I.-J. Hung, H.-C. Liu, T.-H. Jaing, L.-Y. Wang, T.-C. Yeh, Cooperating mutations of receptor kinases and Ras genes in childhood core-binding factor acute myeloid leukemia and a comparative analysis on paired diagnosis and relapse samples. *Leukemia* **22**, 303–307 (2008).

27. M. Ibáñez, J. Carbonell-Caballero, E. Such, L. García-Alonso, A. Liquori, M. López-Pavía, M. Llop, C. Alonso, E. Barragán, I. Gómez-Seguí, A. Neef, D. Hervás, P. Montesinos, G. Sanz, M. A. Sanz, J. Dopazo, J. Cervera, The modular network structure of the mutational landscape of acute myeloid leukemia. *PLOS ONE* **13**, e0202926 (2018).

28. F. Xu, L. Y. Wu, C. K. Chang, Q. He, Z. Zhang, L. Liu, W. H. Shi, J. Guo, Y. Zhu, Y. S. Zhao, S. C. Gu, C. M. Fei, D. Wu, L. Y. Zhou, J. Y. Su, L. X. Song, C. Xiao, X. Li, Whole-exome and targeted sequencing identify *ROBO1* and *ROBO2* mutations as progression-related drivers in myelodysplastic syndromes. *Nat. Commun.* **6**, 8806 (2015).

29. V. Grossmann, E. Tiacci, A. B. Holmes, A. Kohlmann, M. P. Martelli, W. Kern, A. Spanhol-Rosseto, H. U. Klein, S. Schindela, V. Trifonov, S. Schnittger, C. Haferlach, R. Bassan, V. A. Wells, O. Spinelli, J. Chan, R. Rossi, S. Baldoni, L. de Carolis, K. Goetze, H. Serve, R. Peceny, K. A. Kreuzer, D. Oruzio, G. Specchia, F. di Raimondo, F. Fabbiano, M. Sborgia, A. Liso, L. Farinelli, A. Rambaldi, L. Pasqualucci, R. Rabadan, T. Haferlach, B. Falini, Whole-exome sequencing identifies somatic mutations of *BCOR* in acute myeloid leukemia with normal karyotype. *Blood* **118**, 6153–6163 (2011).

30. A. Pellagatti, M. Fernandez-Mercado, C. di Genua, M. J. Larrayoz, S. Killick, H. Dolatshad, A. Burns, M. J. Calasanz, A. Schuh, J. Boultwood, Whole-exome sequencing in del (5q) myelodysplastic syndromes in transformation to acute myeloid leukemia. *Leukemia* **28**, 1148–1151 (2014).

31. J. W. Tyner, C. E. Tognon, D. Bottomly, B. Wilmot, S. E. Kurtz, S. L. Savage, N. Long, A. R. Schultz, E. Traer, M. Abel, A. Agarwal, A. Blucher, U. Borate, J. Bryant, R. Burke, A. Carlos, R. Carpenter, J. Carroll, B. H. Chang, C. Coblentz, A. d'Almeida, R. Cook, A. Danilov, K. H. T. Dao, M. Degnin, D. Devine, J. Dibb, D. K. Edwards V, C. A. Eide, I. English, J. Glover, R. Henson, H. Ho, A. Jemal, K. Johnson, R. Johnson, B. Junio, A. Kaempf, J. Leonard, C. Lin, S. Q. Liu, P. Lo, M. M. Loriaux, S. Luty, T. Macey, J. MacManiman, J. Martinez, M. Mori, D. Nelson, C. Nichols, J. Peters, J. Ramsdill, A. Rofelty, R. Schuff, R. Searles, E. Segerdell, R. L. Smith, S. E. Spurgeon, T. Sweeney, A. Thapa, C. Visser, J. Wagner, K. Watanabe-Smith, K. Werth, J. Wolf, L. White, A. Yates, H. Zhang, C. R. Cogle, R. H. Collins, D. C. Connolly, M. W. Deininger, L. Drusbosky, C. S. Hourigan, C. T. Jordan, P. Kropf, T. L. Lin, M. E. Martinez, B. C. Medeiros, R. R. Pallapati, D. A. Pollyea, R. T. Swords, J. M. Watts, S. J. Weir, D. L. Wiest, R. M. Winters, S. K. McWeeney, B. J. Druker, Functional genomic landscape of acute myeloid leukaemia. *Nature* **562**, 526–531 (2018).

32. T. Okeyo-Owuor, Y. Li, R. M. Patel, W. Yang, E. B. Casey, A. S. Cluster, S. N. Porter, D. Bryder, J. A. Magee, The efficiency of murine MLL-ENL-driven leukemia initiation changes with age and peaks during neonatal development. *Blood Adv.* **3**, 2388–2399 (2019).

33. V. P. Lavallée, I. Baccelli, J. Krosl, B. Wilhelm, F. Barabé, P. Gendron, G. Boucher, S. Lemieux, A. Marinier, S. Meloche, J. Hébert, G. Sauvageau, The transcriptomic landscape and directed chemical interrogation of *MLL*-rearranged acute myeloid leukemias. *Nat. Genet.* **47**, 1030–1037 (2015).

34. L. Huang, T. Y. Wong, R. C. Lin, H. Furthmayr, Replacement of threonine 558, a critical site of phosphorylation of moesin in vivo, with aspartate activates F-actin binding of moesin. Regulation by conformational change. *J. Biol. Chem.* **274**, 12803–12810 (1999).

35. Y. Mei, Y. Wang, P. Kumari, A. C. Shetty, D. Clark, T. Gable, A. D. MacKerell, M. Z. Ma, D. J. Weber, A. J. Yang, M. J. Edelman, L. Mao, A piRNA-like small RNA interacts with and modulates p-ERM proteins in human somatic cells. *Nat. Commun.* **6**, 7316 (2015).

36. R. Vaser, S. Adusumalli, S. N. Leng, M. Sikic, P. C. Ng, SIFT missense predictions for genomes. *Nat. Protoc.* **11**, 1–9 (2016).

37. I. A. Adzhubei, S. Schmidt, L. Peshkin, V. E. Ramensky, A. Gerasimova, P. Bork, A. S. Kondrashov, S. R. Sunyaev, A method and server for predicting damaging missense mutations. *Nat. Methods* **7**, 248–249 (2010).

38. H. A. Shihab, J. Gough, M. Mort, D. N. Cooper, I. N. M. Day, T. R. Gaunt, Ranking non-synonymous single nucleotide polymorphisms based on disease concepts. *Hum. Genomics* **8**, 11 (2014).

39. K. Kitano, F. Yusa, T. Hakoshima, Structure of dimerized radixin FERM domain suggests a novel masking motif in C-terminal residues 295-304. *Acta Crystallogr. Sect. F Struct. Biol. Cryst. Commun.* **62**, 340–345 (2006).

40. R. Viswanatha, J. Wayt, P. Y. Ohouo, M. B. Smolka, A. Bretscher, Interactome analysis reveals ezrin can adopt multiple conformational states. *J. Biol. Chem.* **288**, 35437–35451 (2013).

41. L. Steelman, R. A. Franklin, S. L. Abrams, W. Chappell, C. R. Kempf, J. Bäsecke, F. Stivala, M. Donia, P. Fagone, F. Nicoletti, M. Libra, P. Ruvolo, V. Ruvolo, C. Evangelisti, A. M. Martelli, J. A. McCubrey, Roles of the Ras/Raf/MEK/ERK pathway in leukemia therapy. *Leukemia* **25**, 1080–1094 (2011).

42. K. H. Metzeler, N. Sandhöfer, T. Hinrichsen, E. Zellmeier, B. Ksienzyk, A. Dufour, S. Schneider, P. M. Kakadia, P. A. Greif, M. S. Subklewe, Analysis of cooperating genetic events in MLLT3-MLL rearranged acute myeloid leukemia (AML) by targeted next-generation sequencing of 16 leukemia-related genes reveals frequent mutations affecting growth factor signalling pathways and provides evidence for clonal heterogeneity. *Blood* **120**, 1379 (2012).

43. Cancer Genome Atlas Research Network, Genomic and epigenomic landscapes of adult de novo acute myeloid leukemia. *N. Engl. J. Med.* **368**, 2059–2074 (2013).

44. R. Ono, H. Kumagai, H. Nakajima, A. Hishiya, T. Taki, K. Horikawa, T. Katsu, T. Satoh, Y. Hayashi, T. Kitamura, T. Nosaka, Mixed-lineage-leukemia (MLL) fusion protein collaborates with Ras to induce acute leukemia through aberrant Hox expression and Raf activation. *Leukemia* **23**, 2197–2209 (2009).

45. S. Dutta, A. Krause, S. Vosberg, T. Herold, B. Ksienzyk, L. Quintanilla-Martinez, B. Tizazu, M. Chopra, A. Graf, S. Krebs, H. Blum, P. A. Greif, A. Vetter, K. Metzeler, M. Rothenberg-Thurley, M. R. Schneider, M. Dahlhoff, K. Spiekermann, U. Zimber-Strobl, E. Wolf, S. K. Bohlander, The target cell of transformation is distinct from the leukemia stem cell in murine CALM/AF10 leukemia models. *Leukemia* **30**, 1166–1176 (2016).

46. W. T. Lankes, H. Furthmayr, Moesin: A member of the protein 4.1-talin-ezrin family of proteins. *Proc. Natl. Acad. Sci. U.S.A.* **88**, 8297–8301 (1991).

47. A. Shcherbina, A. Bretscher, D. M. Kenney, E. Remold-O'Donnell, Moesin, the major ERM protein of lymphocytes and platelets, differs from ezrin in its insensitivity to calpain. *FEBS Lett.* **443**, 31–36 (1999).

48. J. Clucas, F. Valderrama, ERM proteins in cancer progression. *J. Cell Sci.* **127**, 267–275 (2014).

49. H. Kobayashi, J. Sagara, H. Kurita, M. Morifuji, M. Ohishi, K. Kurashina, S. Taniguchi, Clinical significance of cellular distribution of moesin in patients with oral squamous cell carcinoma. *Clin. Cancer Res.* **10**, 572–580 (2004).

50. A. Estecha, L. Sánchez-Martín, A. Puig-Kröger, R. A. Bartolomé, J.. Teixidó, R. Samaniego, P. Sánchez-Mateos, Moesin orchestrates cortical polarity of melanoma tumour cells to initiate 3D invasion. *J. Cell Sci.* **122**, 3492–3501 (2009).

51. Y. Qin, W. Chen, G. Jiang, L. Zhou, X. Yang, H. Li, X. He, H.-L. Wang, Y.-B. Zhou, S. Huang, S. Liu, Interfering MSN-NONO complex–activated CREB signaling serves as a therapeutic strategy for triple-negative breast cancer. *Sci. Adv.* **6**, eaaw9960 (2020).

52. F. Tort, M. Pinyol, K. Pulford, G. Roncador, L. Hernandez, I. Nayach, H. C. Kluin-Nelemans, P. Kluin, C. Touriol, G. Delsol, D. Mason, E. Campo, Molecular characterization of a new ALK translocation involving moesin (MSN-ALK) in anaplastic large cell lymphoma. *Lab. Invest.* **81**, 419–426 (2001).

53. C. Lagresle-Peyrou, S. Luce, F. Ouchani, T. S. Soheili, H. Sadek, M. Chouteau, A. Durand, I. Pic, J. Majewski, C. Brouzes, N. Lambert, A. Bohineust, E. Verhoeyen, F.-L. Cosset, A. Magerus-Chatinet, F. Rieux-Laucat, V. Gandemer, D. Monnier, C. Heijmans, M. van Gijn, V. A. Dalm, N. Mahlaoui, J.-L. Stephan, C. Picard, A. Durandy, S. Kracker, C. Hivroz, N. Jabado, G. de Saint Basile, A. Fischer, M. Cavazzana, X-linked primary immunodeficiency associated with hemizygous mutations in the moesin (MSN) gene. *J. Allergy Clin. Immunol.* **138**, 1681–1689.e8 (2016).

54. X. Liu, T. Yang, K. Suzuki, S. Tsukita, M. Ishii, S. Zhou, G. Wang, L. Cao, F. Qian, S. Taylor, M. J. Oh, I. Levitan, R. D. Ye, G. K. Carnegie, Y. Zhao, A. B. Malik, J. Xu, Moesin and myosin phosphatase confine neutrophil orientation in a chemotactic gradient. *J. Exp. Med.* **212**, 267–280 (2015).

55. B. Mizukawa, E. O'Brien, D. C. Moreira, M. Wunderlich, C. L. Hochstetler, X. Duan, W. Liu, E. Orr, H. L. Grimes, J. C. Mulloy, Y. Zheng, The cell polarity determinant CDC42 controls division symmetry to block leukemia cell differentiation. *Blood* **130**, 1336–1346 (2017).

56. P. Zhang, L. Azizi, S. Kukkurainen, T. Gao, M. Baikoghli, M. C. Jacquier, Y. Sun, J. A. E. Määttä, R. H. Cheng, B. Wehrle-Haller, V. P. Hytönen, J. Wu, Crystal structure of the FERM-folded talin head reveals the determinants for integrin binding. *Proc. Natl. Acad. Sci. U.S.A.* **117**, 32402–32412 (2020).

57. E. Weisberg, C. Meng, A. Case, M. Sattler, H. L. Tiv, P. C. Gokhale, S. Buhrlage, J. Wang, N. Gray, R. Stone, S. Liu, S. V. Bhagwat, R. V. Tiu, S. Adamia, J. D. Griffin, Evaluation of ERK as a therapeutic target in acute myelogenous leukemia. *Leukemia* **34**, 625–629 (2020).

58. K. J. Geißler, M. J. Jung, L. B. Riecken, T. Sperka, Y. Cui, S. Schacke, U. Merkel, R. Markwart, I. Rubio, M. E. Than, C. Breithaupt, S. Peuker, R. Seifert, U. B. Kaupp, P. Herrlich, H. Morrison, Regulation of Son of sevenless by the membrane-actin linker protein ezrin. *Proc. Natl. Acad. Sci.* **110**, 20587–20592 (2013).

59. T. Sperka, K. J. Geißler, U. Merkel, I. Scholl, I. Rubio, P. Herrlich, H. L. Morrison, Activation of Ras requires the ERM-dependent link of actin to the plasma membrane. *PLOS ONE* **6**, e27511 (2011).

60. W. S. Pear, J. P. Miller, L. Xu, J. C. Pui, B. Soffer, R. C. Quackenbush, A. M. Pendergast, R. Bronson, J. C. Aster, M. L. Scott, D. Baltimore, Efficient and rapid induction of a chronic myelogenous leukemia-like myeloproliferative disease in mice receiving P210 bcr/abl-transduced bone marrow. *Blood* **92**, 3780–3792 (1998).

61. C. Fellmann, T. Hoffmann, V. Sridhar, B. Hopfgartner, M. Muhar, M. Roth, D. Y. Lai, I. A. Barbosa, J. S. Kwon, Y. Guan, An optimized microRNA backbone for effective single-copy RNAi. *Cell reports* **5**, 1704–1713 (2013).

62. G. A. Van der Auwera, M. O. Carneiro, C. Hartl, R. Poplin, G. D. Angel, A. Levy-Moonshine, T. Jordan, K. Shakir, D. Roazen, J. Thibault, E. Banks, K. V. Garimella, D. Altshuler, S. Gabriel, M. A. De Pristo, From FastQ data to high-confidence variant calls: The genome analysis toolkit best practices pipeline. *Curr. Protoc. Bioinformatics* **43**, 11.10.11–11.10.33 (2013).

63. H. Li, Aligning sequence reads, clone sequences and assembly contigs with BWA-MEM. arXiv:1303.3997 [q-bio.GN] (2013).

64. H. Li, B. Handsaker, A. Wysoker, T. Fennell, J. Ruan, N. Homer, G. Marth, G. Abecasis, R. Durbin; 1000 Genome Project Data Processing Subgroup, The sequence alignment/map format and SAMtools. *Bioinformatics* **25**, 2078–2079 (2009).

65. A. McKenna, M. Hanna, E. Banks, A. Sivachenko, K. Cibulskis, A. Kernytsky, K. Garimella, D. Altshuler, S. Gabriel, M. Daly, M. A. DePristo, The Genome Analysis Toolkit: A MapReduce framework for analyzing next-generation DNA sequencing data. *Genome Res.* **20**, 1297–1303 (2010).

66. Y. Choi, A. P. Chan, PROVEAN web server: A tool to predict the functional effect of amino acid substitutions and indels. *Bioinformatics* **31**, 2745–2747 (2015).

67. B. Webb, A. Sali, Comparative protein structure modeling using MODELLER. *Curr. Protoc. Protein Sci.* **86**, 2.9.1–2.9.37 (2016).

68. S. C. Lovell, I. W. Davis, W. B. Arendall III, P. I. W. de Bakker, J. M. Word, M. G. Prisant, J. S. Richardson, D. C. Richardson, Structure validation by Cα geometry: ϕ,ψ and Cβ deviation. *Proteins* **50**, 437–450 (2003).

69. W. R. P. Scott, P. H. Hünenberger, I. G. Tironi, A. E. Mark, S. R. Billeter, J. Fennen, A. E. Torda, T. Huber, P. Krüger, W. F. van Gunsteren, The GROMOS biomolecular simulation program package. *Chem. A Eur. J.* **103**, 3596–3607 (1999).

70. J. Cox, M. Mann, MaxQuant enables high peptide identification rates, individualized p.p.b.-range mass accuracies and proteome-wide protein quantification. *Nat. Biotechnol.* **26**, 1367–1372 (2008).

71. J. Cox, N. Neuhauser, A. Michalski, R. A. Scheltema, J. V. Olsen, M. Mann, Andromeda: A peptide search engine integrated into the MaxQuant environment. *J. Proteome Res.* **10**, 1794–1805 (2011).

Science Advances

A somatic mutation in moesin drives progression into acute myeloid leukemia

Ouyang Yuan, Amol Ugale, Tommaso de Marchi, Vimala Anthonydhason, Anna Konturek-Ciesla, Haixia Wan, Mohamed Eldeeb, Caroline Drabe, Maria Jassinskaja, Jenny Hansson, Isabel Hidalgo, Talia Velasco-Hernandez, Jrg Cammenga, Jeffrey A. Magee, Emma Nimus, and David Bryder

View the article online
https://www.science.org/doi/10.1126/sciadv.abm9987
Permissions
https://www.science.org/help/reprints-and-permissions

Use of this article is subject to the Terms of service